

Electron Structures in Titan's Induced Magnetosphere and Low-Frequency Wave Activity



Key Points:

- The quasi-periodic plasma structures were observed during the T36 Cassini Titan flyby when Titan was in Saturn's noon magnetosphere
- The importance of local plasma processes at the boundaries, for example, wave generation mechanisms, is assessed in Titan's induced magnetosphere
- The discussed processes highlight the importance of the coupling between large-scale and local plasma processes

Correspondence to:

K. Kim,
konstantin.kim@irfu.se

Citation:

Kim, K., Edberg, N. J. T., Modolo, R., Morooka, M., Wilson, R. J., Coates, A. J., et al. (2025). Electron structures in Titan's induced magnetosphere and low-frequency wave activity. *Journal of Geophysical Research: Planets*, 130, e2024JE008802. <https://doi.org/10.1029/2024JE008802>














Received 21 OCT 2024
Accepted 5 MAY 2025

Author Contributions:

Conceptualization: Konstantin Kim, Niklas J. T. Edberg, Michiko Morooka
Data curation: Konstantin Kim, Niklas J. T. Edberg, R. J. Wilson, Andrew J. Coates, Anne Wellbrock
Formal analysis: Konstantin Kim, Niklas J. T. Edberg, Ronan Modolo, Michiko Morooka, R. J. Wilson, Andrew J. Coates, Anne Wellbrock, Jan-Erik Wahlund, Erik Vigren, Ali Sulaiman, Cesar Bertucci
Funding acquisition: Niklas J. T. Edberg
Investigation: Konstantin Kim, Niklas J. T. Edberg, Ronan Modolo, Michiko Morooka, R. J. Wilson, Andrew J. Coates, Anne Wellbrock, Jan-Erik Wahlund, Ali Sulaiman, Cesar Bertucci, Ravindra Desai, Leonardo Regoli
Methodology: Konstantin Kim, Niklas J. T. Edberg, Ronan Modolo, R. J. Wilson, Andrew J. Coates, Anne Wellbrock

© 2025. The Author(s).

This is an open access article under the terms of the [Creative Commons Attribution License](https://creativecommons.org/licenses/by/4.0/), which permits use, distribution and reproduction in any medium, provided the original work is properly cited.

Konstantin Kim^{1,2} , Niklas J. T. Edberg¹ , Ronan Modolo³ , Michiko Morooka¹ , R. J. Wilson⁴ , Andrew J. Coates^{5,6} , Anne Wellbrock^{5,6} , Jan-Erik Wahlund¹ , Erik Vigren¹ , Ali Sulaiman⁷ , Cesar Bertucci^{8,9} , Ravindra Desai¹⁰ , and Leonardo Regoli¹¹ 

¹Swedish Institute of Space Physics, Uppsala, Sweden, ²Department of Physics and Astronomy, Uppsala University, Uppsala, Sweden, ³LATMOS/CNRS, Sorbonne Université, UVSQ, Paris, France, ⁴Laboratory of Atmospheric and Space Physics, University of Colorado, Boulder, CO, USA, ⁵Mullard Space Science Laboratory, University College London, Dorking, UK, ⁶Centre for Planetary Sciences at UCL/Birkbeck, London, UK, ⁷School of Physics and Astronomy, Minnesota Institute for Astrophysics, University of Minnesota, Minneapolis, MN, USA, ⁸IAFE, UBA CONICET, Buenos Aires, Argentina, ⁹Department of Physics, FCEyN, UBA, Buenos Aires, Argentina, ¹⁰Centre for Fusion, Space & Astrophysics, University of Warwick, Coventry, UK, ¹¹Applied Physics Laboratory, John Hopkins University, Laurel, MD, USA

Abstract The interaction of Titan's ionosphere with Saturn's magnetosphere leads to a mix of perturbed electromagnetic fields and accelerated and thermalized plasma in the induced magnetosphere. The complexity of this region has been noted in previous studies. However, many local structures and processes have not been studied and addressed in detail before. In this case study, we examine the origin of quasi-periodic plasma structures in Titan's induced magnetosphere observed during the T36 flyby. We use data from the electron and ion spectrometers CAPS/ELS and IMS, the RPWS Langmuir probe and electric antenna, and the fluxgate magnetometer (MAG) to analyze plasma parameters, for example, density and temperature and magnetic field fluctuations, to characterize the processes involved. The observed plasma structures are quasi-periodic on a scale of about 20 s (or local ion gyroperiod) and possess acceleration signatures from a few eV up to 700 eV. A burst of low-frequency (around the ion-cyclotron and lower-hybrid frequency) and low-amplitude ($B_{bg} \approx 7$ nT, $\delta B/B_{bg} \approx 0.14$) waves are observed in the proximity of the plasma structures. We discuss possible mechanisms leading to the development of the observed plasma structures, for example, magnetohydrodynamics instabilities and the contribution of the local electric fields.

Plain Language Summary The magnetic field of Saturn heavily influences the dynamics of Titan's plasma environment. While the large-scale interaction has been addressed via simulations and observations in previous studies, some local properties and physical processes in Titan's plasma environment are still not understood. In this study, using Cassini's plasma and field instruments we investigate quasi-periodic structures observed during the T36 flyby. We find that the structures have acceleration signatures and are accompanied by low-frequency wave activity. The observations reported in this paper have not been identified in previous studies. They are important as the explanation couples the large-scale dynamics of Saturn's magnetic field and local properties of plasma and fields in Titan's environment.

1. Introduction

Titan is the largest moon of Saturn (1 Titan radius $R_T = 2574.7$ km), orbiting the planet at a distance of $\sim 20 R_S$ (1 Saturn radius $R_S = 60268$ km). An intrinsic magnetic field of Titan has not been confirmed (not detected or is rather weak) (e.g., Backes et al., 2005; Wei et al., 2010). The atmosphere of Titan consists of predominantly molecular nitrogen N_2 and methane CH_4 (e.g., Vuitton et al., 2007; Waite et al., 2005). The impinging energetic magnetospheric particles and solar extreme ultraviolet radiation ionize the neutral atmosphere, initiating the complex organic chemistry and ionospheric dynamics. The main ionospheric peak is located at around 950 km and the peak electron density is $\approx 3000 - 3500$ cm^{-3} on the dayside (the solar zenith angle/SZA $< 90^\circ$) and on the nightside the peak electron density is $500 - 1000$ cm^{-3} (Ågren et al., 2009). The influence of transverse to the magnetic field currents (Pedersen and Hall currents) in Titan's ionosphere has the most effect at $1,450 \pm 95$ km altitude (Rosenqvist et al., 2009). The topside ionosphere of Titan is influenced by its position relative to Saturn's plasma sheet (e.g., Kabanovic et al., 2017; Simon et al., 2010, 2013). In addition, Titan's orbit is close to Saturn's

Project administration: Konstantin Kim, Niklas J. T. Edberg

Resources: Konstantin Kim, Niklas J. T. Edberg

Software: Konstantin Kim, Michiko Morooka, Ravindra Desai

Supervision: Niklas J. T. Edberg, Jan-Erik Wahlund, Erik Vigren

Validation: Konstantin Kim, Niklas J. T. Edberg, Ronan Modolo, R. J. Wilson, Andrew J. Coates, Anne Wellbrock, Erik Vigren, Ali Sulaiman, Ravindra Desai, Leonardo Regoli

Visualization: Konstantin Kim, Niklas J. T. Edberg

Writing – original draft:

Konstantin Kim, Niklas J. T. Edberg

Writing – review & editing:

Konstantin Kim, Niklas J. T. Edberg, Ronan Modolo, Michiko Morooka, R. J. Wilson, Andrew J. Coates, Anne Wellbrock, Jan-Erik Wahlund, Erik Vigren, Ali Sulaiman, Cesar Bertucci, Ravindra Desai, Leonardo Regoli

subsolar magnetopause, and when Saturn's dayside magnetosphere is disturbed, for example, due to an increase in the solar wind's dynamic pressure such as during a coronal mass ejection impact, Titan can be exposed to the shocked magnetosheath plasma or even the solar wind (e.g., Bertucci et al., 2008, 2015; Burne et al., 2023; Edberg et al., 2013; Feyerabend et al., 2016; Omid et al., 2017; Wahlund et al., 2014; Wei et al., 2011).

An induced magnetosphere is a plasma region around unmagnetized bodies resulting from the solar wind or ambient magnetospheric plasma flow interaction with the body's atmosphere. Depending on the upstream flow velocity V , local Alfvén speed V_A and sound speed V_s , the magnetosonic Mach number $M_f = V/\sqrt{V_A^2 + V_s^2}$ can either be less or greater than unity, and the upstream is called either submagnetosonic (e.g., corotating magnetospheric plasma) or super-fast magnetosonic (e.g., solar wind) flow correspondingly. If $M_f > 1$, then the magnetohydrodynamic (MHD) wave—fast-magnetosonic wave—is excited and propagates into an upstream region of an obstacle, creating a bow shock (Kivelson & Russell, 1995). If the interaction leads to the formation of a bow shock, the flow is decelerated, heated, and deflected around the obstacle. Because the obstacle is unmagnetized (there is no intrinsic dipole magnetic field similar to, e.g., Earth), the decelerated and heated plasma flow interacts directly with the ionosphere. As we deal with collisionless plasma, the upstream magnetic field is frozen-in into the plasma and is convected downstream of the shock. However, in Titan's ionosphere due to the ion-neutral collisions the magnetic field is frozen-in into electrons. The magnetic field is bent around an obstacle following the plasma flow when approaching the ionosphere. The induced currents that are created in the ionosphere due to this interaction act to cancel out the convected magnetic field.

The interface between the decelerated and heated plasma flow and perturbed magnetic fields, or magnetic pileup region (MPR), and ionosphere has different names, is called the magnetic pileup boundary (MPB) or induced magnetosphere boundary (IMB), and is a region where waves and instabilities and plasma loss processes (non-thermal losses) develop. If the upstream flow is submagnetosonic, a bow shock will not form and other mechanisms become important in the deceleration, heating, and deflection of a plasma flow. The newly formed ions play a significant role, as they are picked up by the upstream flow and undergo $\mathbf{E} \times \mathbf{B}$ -drift, and gain kinetic energy from the upstream flow, causing the flow deceleration. The heating is then caused by collisions between the picked-up ions and the collisional ionosphere (if the gyroradius of pick-up ions is $\leq R_T$), and wave-particle interactions. This process is called mass-loading and is important around moons and active comets (e.g., Szegő et al., 2000). The mass-loaded upstream plasma flow is decelerated and deflected around the obstacle. Similarly, the magnetic field is shielded due to ionospheric currents and bent around the moon. The mass-loading effects are important above the exobase, whereas the ion-neutral collisions play a bigger role in the flow deceleration below the exobase.

The induced magnetosphere of Titan lacks continuous observations, however, it was observed during multiple flybys. The first evidence of an induced magnetosphere around Titan was reported after the Voyager 1 flyby (Ness et al., 1982). After the Voyager 1 flyby, the next spacecraft that visited Titan was Cassini having a total of 127 close flybys from 2004 until the end of the mission in 2017. The data from the first Cassini's Titan flyby, TA in 2004, was analyzed by Backes et al. (2005). The long magnetic diffusion times (order of hours) within a large-scale ionosphere lead to a unique feature of Titan's induced magnetosphere—fossilized magnetic fields (Bertucci et al., 2008). Due to this effect, there are multiple layers of differently oriented magnetic fields “memorized” by the ionosphere. Chen and Simon (2020) conducted a statistical study of the induced magnetosphere of Titan. The asymmetry between the Saturn-side and anti-Saturn-side of the induced magnetosphere was related to the gyromotion of ions. The lower boundary of the induced magnetosphere or magnetic pile-up region was located at $0.35 R_T$ (964 km) on average and the radial profile of the magnetic field did not depend on the orbital phase. The orientation of the dayside ionosphere was shown to have a second-order effect on a general interaction pattern but might have a local influence on Titan's ionosphere and the local energy balance (Ledvina et al., 2012).

Despite the wide range of processes requiring collisionless energy transfer in Titan's induced magnetosphere, the plasma wave activity around Titan is poorly understood. Prior to the arrival of Cassini, Dóbbé and Szegő (2005) analyzed linear beam-driven instabilities using hybrid particle-in-cell simulation and a kinetic dispersion relation solver. Two distinct wave modes were found: the non-resonant fluid-like modified two-stream instability and resonant kinetic ion-ion acoustic instability. However, none of the proposed wave modes or instabilities have been observed in situ yet. Another type of instability is driven by the pick-up ions. The pick-up ion distribution is anisotropic in perpendicular to the local magnetic field direction and thus unstable for temperature anisotropy-

driven instabilities, for example, resonant ion cyclotron instability. Pick-up ions were observed at Titan (e.g., Hartle et al., 2006; Regoli et al., 2016), but the ion cyclotron waves were identified only twice during the T63 and T98 flybys (e.g., Cowee et al., 2010; Russell et al., 2016). The role of plasma waves around Titan is largely underexplored, despite the expectations from the simulations (Dóbbé & Szegő, 2005). It may be that the waves are heavily damped or the growth rate for instability is too slow compared with the observation time and convection time.

In this paper, we investigate the physical processes and structure of Titan's induced magnetosphere observed during the T36 flyby. We use data from the plasma spectrometers, electric antennas and probes, and magnetometers (for details see Section 2) to infer the properties of plasma, for example, density and temperature, and the low-frequency fluctuations of the magnetic field. We find quasi-periodic dispersive plasma structures in the IMB of Titan and discuss how they might be connected to the low-frequency wave activity. The paper is structured as follows: in Section 2 the used instruments and methods are described. The T36 flyby trajectory is described in Section 3, followed by the description of the local and ambient plasma environment. In Section 4 we discuss possible driving mechanisms and then conclude the paper in Section 5.

2. Methods

In this section, we describe particle and wave instruments and methods.

2.1. Instrumentation

The Radio and Plasma Waves/Langmuir probe (RPWS/LP) is a 5 cm diameter sphere with titanium-nitride coating mounted on a 1.5 m boom (Gurnett et al., 2004). By sweeping from the positive to negative bias potential of the probe, charged particles are either repelled or attracted to the probe's surface. The resulting current is then fitted using appropriate assumptions, for example, orbital- or sheath-limited theories, providing the electron and ion density and temperature, as well as the spacecraft potential (e.g., Chatain et al., 2021; Gustafsson & Wahlund, 2010; Morooka et al., 2011; Shebanits et al., 2016). The average error of the measurements is about 10%. A sweep is carried out once every 24 s during Titan flybys. To increase the time resolution, the bias-voltage applied to the probe is fixed at a positive value in between each sweep and the resulting electron current, which is proportional to both electron density and electron temperature, is measured. This allows increasing the sampling rate of an electron density up to 20 Hz (later referenced as “20 Hz”) once the sampled current has been calibrated to the sweep-derived density. Another way of obtaining the plasma density is by determining the plasma oscillations in the spectrum of electric fluctuations measured by the electrical antennas. In magnetized plasma, a high-frequency transverse resonance, upper-hybrid resonance, emission band is observed, and the dispersion relation is $f_{UH}^2 = f_{pe}^2 + f_{ce}^2$, where f_{pe} is the electron plasma frequency and f_{ce} is the electron cyclotron frequency. In dense ionospheric plasmas, $f_{pe}^2 \gg f_{ce}^2$, and therefore the electron density (in cm^{-3}) can be estimated as $n_e \approx \left(f_{UH} / \sqrt{e^2 / \pi m_e} \right)^2 \approx (f_{UH} / 8980)^2$.

The electron and ion spectrometers CAPS/ELS and CAPS/IMS (Young et al., 2004) are hemispherical top-hat analyzers consisting of an electrostatic analyzer, and eight separate detector anode plates covering 20° in elevation direction. For mass detection, CAPS/IMS uses the time-of-flight (TOF) section, allowing the separation of masses from 1 to 400 amu with mass resolution $M/\Delta M \sim 8$. The ELS has no TOF section, however, the unexpected measurements of heavy negative ions can provide a rough estimation of their mass per charge using the spacecraft velocity (e.g., Coates et al., 2007). To cover the azimuth direction, the spectrometers were mounted on an actuator, changing its position by $\approx 1^\circ$ per second. The spectrometers can measure electron energies from 0.6 to 28,750 eV with 17% resolution, and ion energies from 1 to 50,280 eV with 17% resolution. The instantaneous azimuth and elevation angles coverage is $8.3^\circ \times 160^\circ$ with $8.3^\circ \times 20^\circ$ resolution for IMS, and $5.2^\circ \times 160^\circ$ with $5.2^\circ \times 20^\circ$ resolution for ELS. The combined CAPS/ELS and RPWS/LP measurements provide continuous measurements of the electron density and temperature in both Titan's ionosphere and Saturn's magnetosphere. However, there are limitations one should be aware of. In particular, the RPWS/LP measurements are reliable in dense ($n_e > 1\text{--}10 \text{ cm}^{-3}$), cold ($T_e < 10 \text{ eV}$) ionospheric plasmas as hot and tenuous magnetospheric plasma is insensitive to an electric field of a probe. Therefore, the measurements in Saturn's magnetosphere are provided by the CAPS/ELS. On the other hand, in very dense environments such as Titan's

ionosphere, the spacecraft can become negatively charged, which can affect the lowest energy part of the electron distribution measured by CAPS/ELS.

Finally, the fluxgate magnetometer MAG (M. K. Dougherty et al., 2004) measures the full magnetic field vector with a 32 Hz cadence. Although the magnetometer is mounted halfway of an 11-m boom, the low-frequency noise from the spacecraft itself is visible in the data and must be taken into account (see Section 3.5). In Section 3.5 we apply a wavelet transform to infer the type of the observed magnetic field fluctuations.

2.2. Minimum Variance Analysis Method

The minimum variance analysis method (MVA) is a numerical method for determining the wave properties such as a wave vector \mathbf{k} or a normal direction to plasma discontinuities from a single spacecraft measurements (Sonnerup & Scheible, 1998). The method is based on the calculation of eigenvectors and eigenvalues of the magnetic field variance matrix $\mathbf{M}_{ij} = \langle B_i B_j \rangle - \langle B_i \rangle \langle B_j \rangle$, where i, j indices run through x, y, z-components of the magnetic field B_i . The eigenvector corresponding to the minimum eigenvalue (variance of the magnetic field) shows the direction normal to the discontinuity or parallel to the wave vector \mathbf{k} . The determination of the minimal variance direction is valid if the intermediate to minimum eigenvalue ratio λ_2/λ_3 is large, for example, $\lambda_2/\lambda_3 \geq 3$ (Knetter et al., 2004). If the requirement is satisfied, the magnetic field vector rotates in a maximum-intermediate variance plane. The maximum to intermediate eigenvalues ratio λ_1/λ_2 characterizes the polarization of a wave, for example, $\lambda_1/\lambda_2 = 1$ means that the wave polarization is circular. An important limitation of the MVA method is the uncertainty in determining the sign of the wave vector k . The sign of the wave vector can be determined by imposing additional observations or assumptions, for example, measuring the phase speed of waves.

3. Observations and Analysis

3.1. Reference Frames

We use the local Titan Interaction system (TIIS) and ecliptical reference frames to show the trajectory of Cassini during the T36 flyby and the orientation of the magnetic field with respect to Titan. The TIIS reference frame is based on the right-handed Kronocentric RTP (KRTP), where \mathbf{R} (\mathbf{r}) is directed from Saturn to the spacecraft, \mathbf{P} (ϕ) is directed parallel to Saturn's equator in the corotation direction and \mathbf{T} (θ) completes the right-handed set, roughly directed southward. In TIIS, the \mathbf{x} -axis is along the ideal corotation direction or parallel to ϕ ($x \parallel \phi$), \mathbf{z} -axis is parallel to Saturn's spin axis (anti-parallel to θ ($z \parallel -\theta$)), and the \mathbf{y} -axis completes the right-handed set, being approximately anti-parallel to the radial direction ($y \parallel -r$) and pointing in Saturn's direction. In the Titan-centered reference frame the \mathbf{x} -axis is pointing to the Sun, the \mathbf{z} -axis is given by the cross product of Saturn's orbital direction with \mathbf{x} (approximately perpendicular to the ecliptic plane) and the \mathbf{y} -axis completes the right-hand set, approximately against the orbital motion of Saturn.

3.2. Cassini Trajectory During the T36 Flyby

The T36 flyby trajectory in Titan's vicinity is shown in Figure 1 in two reference frames: (a–c) Titan interaction system (TIIS) and (d) Saturn-centered frames (x -axis pointing to the Sun). During the flyby, Cassini was moving from the wakeside to the ramside of Titan, and from the nightside to the dayside. The closest approach of 973 km was around 04:43 UTC 2007/10/02. The spacecraft velocity v_{SC} with respect to Titan throughout the flyby was $\sim 6 \text{ km s}^{-1}$. During the outbound leg, the measurements of prime interest were conducted at 04:50–05:00 UTC and are highlighted in orange. The estimated distance from the region of interest to the first magnetopause crossing was $v_{SC} \Delta t \approx 3\text{--}4 R_T$. The flyby occurred when Titan was in the noon sector (Saturn Local Time/SLT ~ 11.51) of Saturn's dayside magnetosphere. Figure 1d shows the color-coded timeline of Cassini's trajectory from a few days before and after the T36 flyby. The green cross shows the closest approach, while red and black correspond to the multiple magnetopause (MP) and bow shock (BS) positions. The magnetopause position (red dashed line) was fitted first using the empirical model by Kanani et al. (2010) thereby estimating the upstream dynamic pressure. The estimated upstream dynamic pressure is then used to fit the bow shock position (black dashed line) using the empirical model by Masters et al. (2008). The discrepancy in the fitted and observed bow shock location is probably due to the varying upstream solar wind. This assumption is also supported by the multiple crossings of the magnetopause. During the T36 flyby, Cassini was passing from Saturn's magnetosphere into the magnetosheath and crossed the magnetopause twice: the first time Cassini crossed it at 2007/10/02 05:21

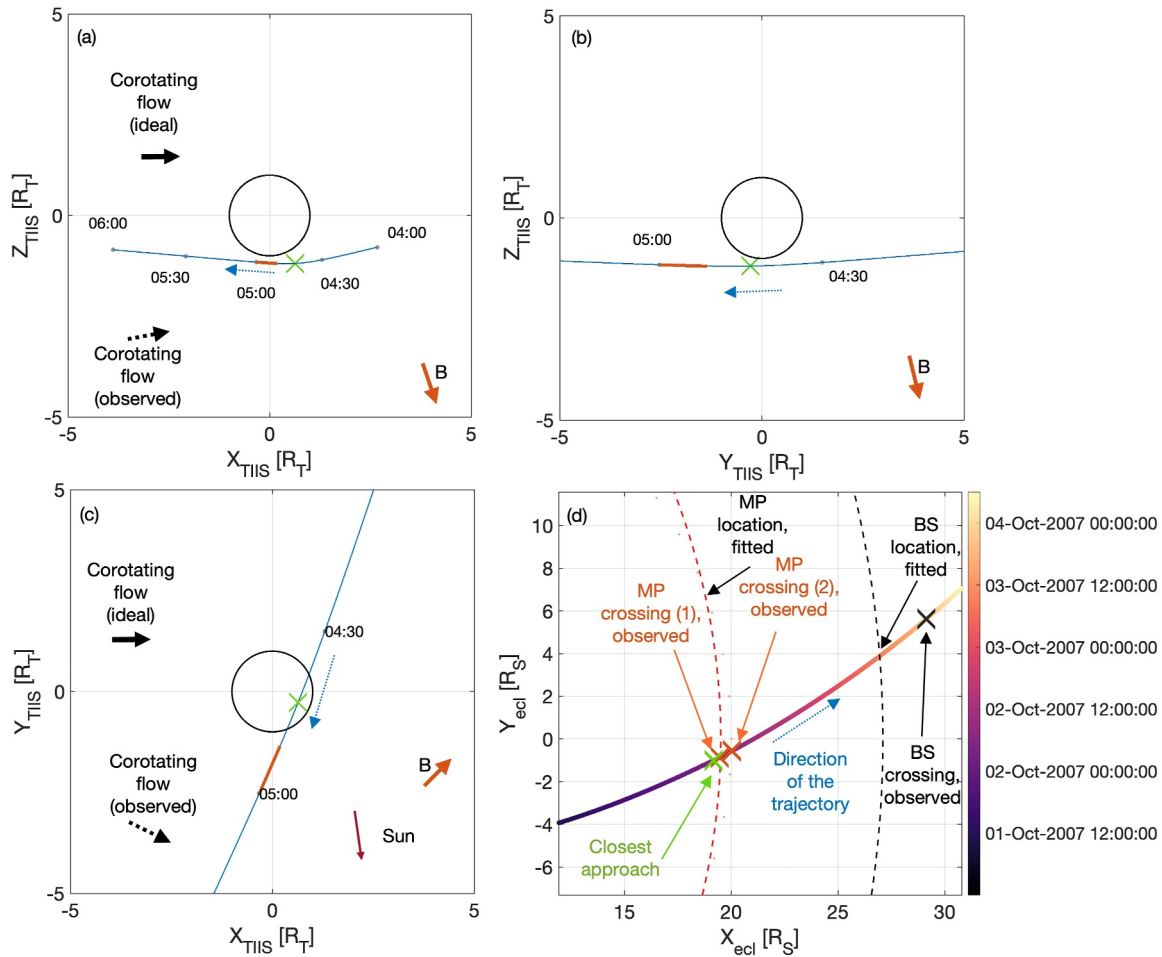


Figure 1. The Cassini's flyby overview trajectory during the T36 in (a–c) Titan interaction system (TIIS) and (d) Saturn-centered reference frame. In panels (a–c), the three projections of the Cassini trajectory are shown. On the blue line (Cassini's trajectory) the region of interest in this study is highlighted in orange. In panel (d) the black and red dashed lines are fitted Saturn's bow shock (BS) and magnetopause (MP) locations. We also indicate with crosses the observed BS (black) and MP (red) positions, and the T36 flyby closest approach (green). The blue dotted arrows show the direction of the trajectory. The orange arrows in panels (a–c) show the projection of the magnetic field. The black solid and dashed arrows in panels (a–c) show the direction of the ideal corotation flow and the observed plasma flow.

to 05:28 UTC, in proximity to Titan ($\approx 5 R_T$); the second time Cassini crossed it around 2007/10/02 07:04 UTC, far away from Titan (at $\approx 19 R_T$).

3.3. An Overview of the T36 Flyby: Plasma and Fields Measurements

In Figure 2 the combined measurements of CAPS IMS/ELS, RPWS LP, and MAG are shown. We use them to identify plasma regions throughout the flyby by analyzing plasma parameters, for example, electron density and temperature, magnetic field direction, and magnitude. According to the classification of the electron and ion spectrum, and magnetic field, during the T36 flyby Titan was located in Saturn's plasma sheet (e.g., Arridge et al., 2011). In the inbound leg at around 04:20–04:30 UTC, the electron density n_e and temperature T_e changed by $\Delta n_e \approx 10^1 - 10^2 \text{ cm}^{-3}$, $\Delta T_e \approx -(10^1 - 10^2) \text{ eV}$ can be seen, indicating the transition from the tenuous plasma in Saturn's magnetosphere into the dense ionosphere of Titan. The electron differential energy flux (DEF) peaked at $\approx 200 \text{ eV}$ and the magnetic field had a magnitude $|B| \approx 5 \text{ nT}$ without significant variations and primarily oriented in the $\mathbf{B}_{z, \text{TIIS}}$ direction. This suggests that during the inbound leg, Cassini was in Saturn's plasma sheet ($n_e \approx 10^{-2} \text{ cm}^{-3}$, $T_e \approx 100 \text{ eV}$) (e.g., Arridge et al., 2011). The same applies to the part of the outbound leg, from 05:00 and onward, with similar plasma and magnetic field parameters. Around 04:37 UTC in the inbound and 04:48 UTC in the outbound legs, a significant localized electron density spike is observed (Kim et al., 2023). The density spike is related to a current sheet observed in the topside ionosphere and has similar properties to an

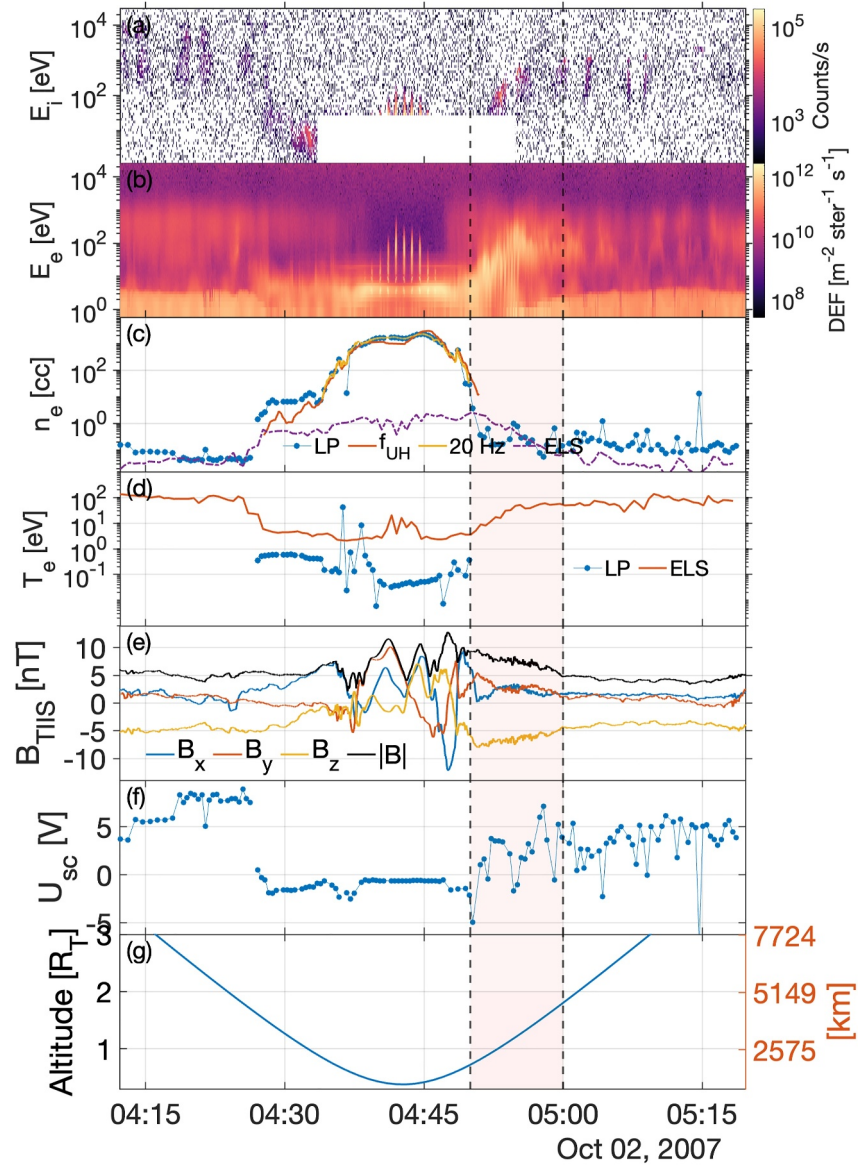


Figure 2. The combined measurements of plasma and fields properties during the T36 flyby: (a, b) ion and electron energy-time spectrogram summed over anodes, ELS data is transformed into differential energy flux (DEF) to account for microchannel plate detector, (c) the electron density calculated from sweeps (blue dash-dotted), upper-hybrid resonance frequency f_{UH} (red), 20 Hz sampling (yellow) and from ELS moments (purple dashed); (d) the electron temperature provided by LP (blue dot-dashed) and ELS (red); (e) the three components of the magnetic field in TiIS reference frame; (f) the spacecraft potential measured by RPWS LP; (g) Cassini's altitude during the T36 flyby. The red-shaded, bounded by a black dashed line, region indicates the time of interest from 04.50 UTC to 05.00 UTC. The gap in the ion measurements during the closest approach is due to the change of energy sweep tables.

ionopause. During the inbound leg, the spacecraft potential measured by RPWS/LP was positive ≈ 8 V, while CAPS/ELS indicates ≈ 4 V as shown by the ELS low energy spectra.

In the time interval around 04:37 UTC to 04:48 UTC, Cassini was in Titan's ionosphere. The closest approach altitude was around 973 km at a solar zenith angle (SZA) of 60° (the angle between the Sun-Titan line and the spacecraft-Titan line). The peak electron density was $\approx 3,000 \text{ cm}^{-3}$ and the electron temperature was $\leq 10^{-1}$ eV. The CAPS/ELS detected negative ions at around the closest approach time, visible in the data as broad energy (from a few eV up to 10^3 eV) bursts as the CAPS actuator scanned through the spacecraft ram direction (e.g., Coates et al., 2007; Desai et al., 2017; Mihailescu et al., 2020; Wellbrock et al., 2013). Around ≈ 20 eV a narrow

beam of cold electrons—ionospheric photoelectrons—was detected from 04:35 UTC until 04:52 UTC (e.g., Coates et al., 2015; Wellbrock et al., 2012). The low-energy electrons (below < 10 eV) are of ionospheric origin. The spacecraft potential during the ionospheric dive was slightly negative, on average ≈ -1.3 V.

Of central importance to this study is the outbound leg, from 04.50 UTC and onward. Similarly to the inbound leg, steep electron density and temperature gradients were observed. In the time interval 04.50–05.00 UTC, the MPR was visible as Cassini passed through the induced magnetosphere on the ramside. There was no significant magnetic field rotation, but the magnitude of the magnetic field changed from ≈ 10 nT at 04.50 UTC to ≈ 5 nT at 05.00 UTC. In the same time interval, low-amplitude magnetic field fluctuations (compared with the background $B_{bg} \approx 7$ nT, $\delta B \approx 1$ nT, $\delta B/B_{bg} \approx 0.14$) were detected. In the ion spectrogram, the presence of narrow ion beams associated with pick-up ions was observed with energies $\approx 400 - 800$ eV. At the same time, the electron spectrogram in the IMB had signatures of modulation and large-scale acceleration from thermal energies ≈ 4 eV up to several hundred eV. The spacecraft potential in the outbound leg in general grows positive from ≈ -2 V to ≈ 5 V, however, is highly variable in the IMB region and beyond in Saturn's magnetosphere, dropping to ≈ -1.7 V at 04.54.40 UTC.

The change in spacecraft potential sign affects the low-energy plasma measurements. In the time interval from 04:28 UTC to 04:51 UTC the spacecraft potential was negative since Cassini was in Titan's ionosphere. In the time interval 04:51 UTC to 04:56 UTC the spacecraft potential was modulated with seemingly the same periodicity as the ionospheric electrons, indicating blobs of electrons that would modulate the spacecraft potential and thus the upper limit of the lowest energy photoelectrons. Finally, in the time interval from 04:56 UTC and onwards, the spacecraft potential was positive as Cassini was entering the magnetosphere. As shown in Figure 2, the presence of spacecraft photoelectrons is a clear sign that the spacecraft potential is positive as it otherwise would have repelled the negative electrons such that they could not have been observed. In the magnetosphere, where nothing prevents the absorption of sunlight by the spacecraft's surface, the photoelectrons are easily emitted. However, when Cassini dived deeper into the ionosphere or dense plasma, the spacecraft potential became negative.

3.4. Fine Structure of Titan's Induced Magnetosphere

In Figure 3 we zoom in on the interval from 04:50 to 05:00 UTC where the unusual plasma signatures mentioned above are observed. The electron spectrogram for each of the eight ELS anodes is shown. The aforementioned modulation of the electron energy spectrum is seen in detail and more pronounced from 04:52 UTC to 04:56 UTC in all anodes. The period T of modulation was ≈ 20 s or had a frequency $f = 1/T \approx 0.05$ Hz. When comparing the modulation frequency with an average local proton cyclotron frequency $f_{pc} = q|B|/2\pi m_p$ in the IMB region (for $|B| = 5 - 10$ nT, $f_{pc} = 0.08 - 0.15$ Hz), it is evident that $f \leq f_{pc}$, and has a large temporal scale, similar to the ion cyclotron frequency. In the top panel (anode 1), the electron populations of various origins are enumerated. The populations (1) and (2) are thermal and accelerated ionospheric electrons indicated by the high DEF ($\geq 10^{11}$ m⁻² ster⁻¹ s⁻¹) and narrow energy distribution with a peak energy starting at 10 eV reaching up to 100 eV. Population (4) is the signature of magnetospheric electrons with peak energy at ≈ 1 keV and temperature ≈ 100 eV, medium DEF ($\approx 10^{10}$ m⁻² ster⁻¹ s⁻¹). The spacecraft-emitted photoelectrons (5) appear in data as a low-energy and low-temperature electron population with a relatively high DEF ($\leq 10^{10}$ - 10^{11} m⁻² ster⁻¹ s⁻¹). The electron “blob” (3) visible around 04:54 UTC is of unknown origin. The blob is observed at low energies (< 10 eV) with a DEF comparable to photoelectrons but had a much larger temperature ≈ 10 eV. The modulation of the electron energy spectrum is most visible in the region with the presence of an electron blob and affects primarily accelerated ionospheric electrons. Notably, the electron blob is not equally visible at all pitch-angles, as can be seen from anodes 3–5 and pitch-angles from 30°–90°. It is worth mentioning, that anodes 1 and 8 are the most affected by the spacecraft-plasma interactions, and anodes 3–6 are the least affected. However, in Figure 3 it is seen that the described above features are consistent in all of the anodes (except for a “blob” population).

In Figure 4 the DEF normalized by the maximum value of DEF for every other energy step with the magnetic field fluctuations δB are shown. We show every other energy level to demonstrate the general pattern without losing any generality of the analysis. The magnetic field fluctuations δB are calculated as a difference between the measured and averaged over a sliding 1-min window magnetic field. The localized increase in fluxes around 04.45 UTC is associated with the negative ions in Titan's ionosphere during the close approach. We observe the apparent increase in the DEF between 04.50 UTC and 05.00 UTC, which happens simultaneously as increased

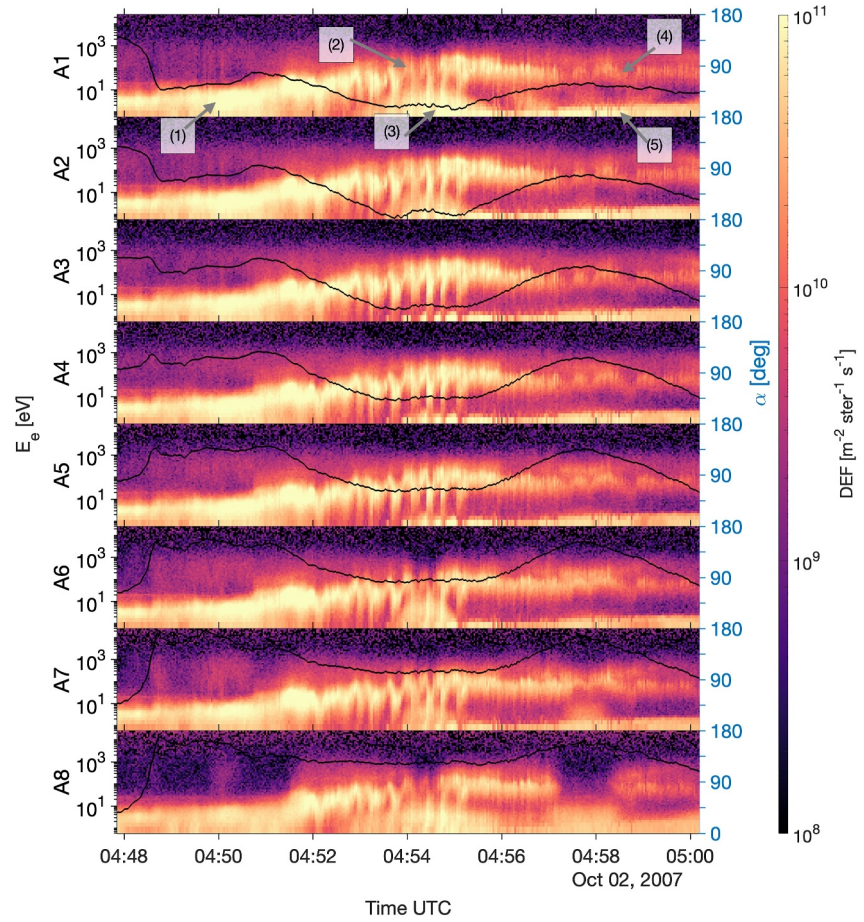


Figure 3. The electron spectrogram (on the left axis) and the instantaneous pitch-angle for each of the ELS anodes A1–A8 (in ascending order from top to bottom). The color scale indicates the differential energy flux (DEF). In Anode 1, a few electron populations are enumerated: (1) ionospheric electrons; (2) electrons accelerated by the upstream convective electric field; (3) the blob of low-energy electrons; (4) the background magnetospheric electrons; (5) the spacecraft photoelectrons.

magnetic field fluctuations. The maximum observed amplitude of the magnetic field fluctuations $\delta B_{\max} \approx 1$ nT. The vertical red and blue lines show which localized peaks of DEF correspond to the positive and negative magnetic field fluctuation change $\overline{\delta B/\delta t}$ averaged over $\delta t = \pm 1$ s interval. There is no clear trend showing that the apparent increase in the DEF is related to either positive or negative changes in the fluctuating magnetic field.

3.5. Magnetic Field Fluctuations: Waves Properties

In Figure 5 the power spectral density averaged over 04.53–05.00 UTC time interval is shown. The background magnetic field $\hat{\mathbf{b}}$ in the IMB region is $\hat{\mathbf{b}} = (0.37 \ 0.31\text{--}0.88)$ and primarily along the $-\hat{\mathbf{z}}$ direction. We thus can assume that $\hat{\mathbf{b}}_{\parallel} \approx -\hat{\mathbf{z}}$, $\hat{\mathbf{b}}_{\perp 1} \approx -\hat{\mathbf{x}}$ and $\hat{\mathbf{b}}_{\perp 2} \approx -\hat{\mathbf{y}}$. In general, the power of transverse magnetic field fluctuations B_{\perp} is larger than compressional component B_{\parallel} at almost all frequencies, expect a narrow band $\approx 10^{-2} - 5 \cdot 10^{-2}$ Hz. The peak in the power spectral density (PSD) around 2–3 Hz range is associated with the noise from the reaction wheels. There are localized peaks in the PSD in both compressional and transverse components of the magnetic field, however, they have somewhat different frequencies. The first peak at $\approx 2 \cdot 10^{-2}$ Hz is present in both compressional and transverse components. The second peak in the transverse component is found at $\approx 4.6 \cdot 10^{-2}$ Hz, while in the compressional component—at $\approx 8 \cdot 10^{-3}$ Hz. However, the peaks are very localized in frequency and the peak values are on the order of $\approx 1 - 10$ nT² Hz⁻¹. We imply that the observed fluctuations are below the ion scale, which means that at such scales in magnetized plasma, one can observe MHD waves, that is, fast and slow magnetosonic (compressional Alfvén) waves and torsional Alfvén waves. The peaks in magnetic field power and the calculated cyclotron frequencies do not correspond to each other perfectly. The

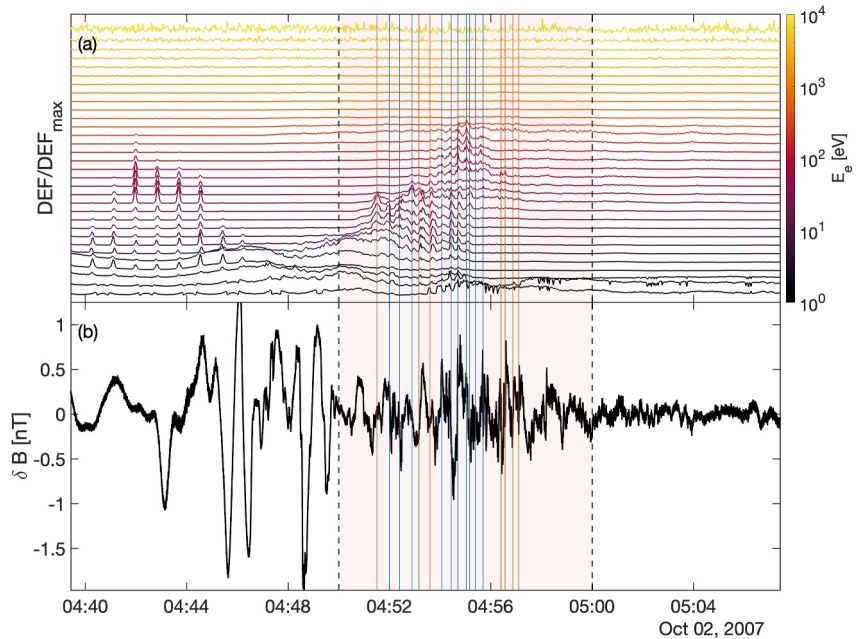


Figure 4. The close-up view on a region between 04.50 and 05.00 UTC (the region is highlighted in red). Panel (a) shows summed over anodes stacked normalized DEF (normalized by the maximum value of DEF) for every other energy step (the energy steps are color-coded). Panel (b) shows the magnetic field fluctuations δB , calculated as the difference between the measured magnetic field and the averaged with sliding 1-min window background magnetic field. The vertical red and blue lines indicate DEF peaks corresponding to $\delta B/\delta t > 0$ and $\delta B/\delta t < 0$, where $\delta t = \pm 1$ s around the localized DEF peak.

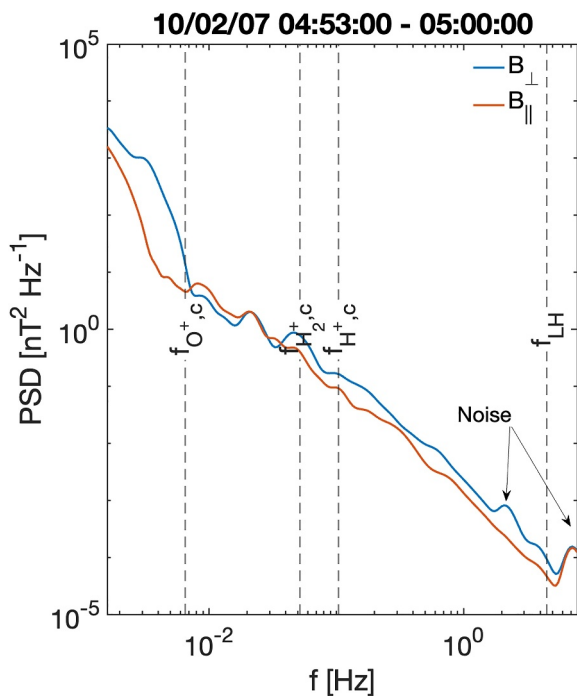


Figure 5. The average power spectral density (PSD), calculated separately for transverse B_{\perp} (blue) and compressional B_{\parallel} (red) components of the magnetic field. The vertical lines indicate the cyclotron frequencies of H^+ , H_2^+ and O^+ ions, and lower-hybrid frequency f_{LH} . The localized peaks in the PSD indicate the interference lines, at $\approx 2 - 3$ Hz and $\approx 7 - 8$ Hz.

shift toward lower frequencies can be explained as a result of averaging over a period where the magnetic field is also changing.

In Figure 6 magnetic field fluctuations in the induced magnetosphere of Titan are shown in different frequency ranges. In panel (a) the magnetic field in the induced magnetospheric region is shown. In panel (b) the wavelet transform of the magnetic field with overlaid cyclotron frequencies of H^+ , H_2^+ and O^+ ions (white solid line) is shown. The maximum frequency of fluctuations is bounded by the Nyquist frequency at 8 Hz. In panels (c) and (d) the bandpass filter was applied on the magnetic field to extract the wave magnetic field. The bandpass window is chosen based on Figure 5. There is an enhancement in magnetic field power at around the proton cyclotron frequency and below the lower-hybrid frequency, peaking at 04:55 UTC.

The fluctuations might occur at the lower frequencies (see Section 4) due to Doppler shift (due to the bulk motions of plasma). In the plasma rest frame, the frequency of the fluctuations f_0 is given by the expression Equation 1 $f_0 = f_{obs} - \mathbf{k} \cdot \mathbf{V}/2\pi$, where \mathbf{V} is a bulk velocity and \mathbf{k} is a wave vector, meaning that one has to estimate the wave vector direction. Assuming that the fluctuations in the plasma rest frame are alfvénic and knowing the dispersion relation $\omega = V_A k$ or $f = kV_A/2\pi$, where V_A is the Alfvén speed. To determine the properties of waves such as wave vector \mathbf{k} and polarization, we apply the minimum variance analysis method for a frequency range $0.016 \text{ Hz} < f < 0.029 \text{ Hz}$ with the results shown in Table 1. We analyze the low-frequency waves in panel (c) in the time interval 04:52–04:56 UTC, where the apparent magnitude of the fluctuations is enhanced, in the frequency range $0.1 \text{ Hz} < f < 0.2 \text{ Hz}$. Due to the field of view limitation, ambient plasma signatures are not observed by CAPS-IMS in this time interval range. We assume that the bulk velocity of plasma in the induced magnetosphere is

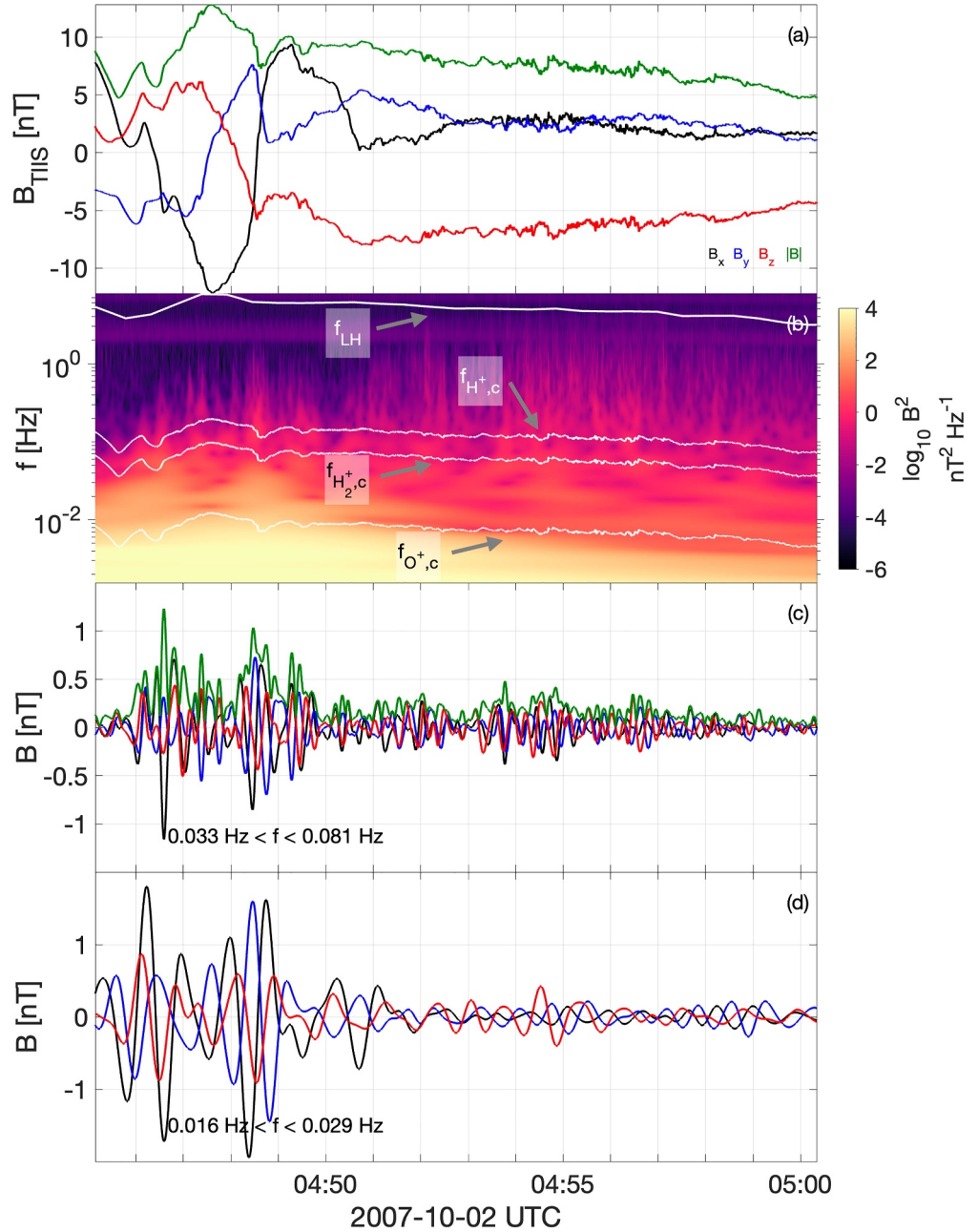


Figure 6. The magnetic field fluctuations in MAG data: (a) the three components of the magnetic field in TIIS reference frame; (b) the Morlet wavelet transform of the magnetic field, the color code represents the power of the fluctuations, the white solid line are cyclotron frequencies of H^+ , H_2^+ and O^+ , and lower-hybrid frequency $f_{LH} = \sqrt{\frac{k_z k_e}{1 + \frac{k_z^2}{k_e^2}} + f_{ci}^2}$; (c) and (d) show the filtered magnetic field $0.033 \text{ Hz} < f < 0.081 \text{ Hz}$ and $0.016 \text{ Hz} < f < 0.029 \text{ Hz}$ frequency ranges. These ranges are chosen so they correspond to the local peaks in the PSD of a wave.

either along the ideal corotation direction or deflected at an angle of $\tan^{-1} V/V_A$ degrees. For upstream parameters taken in the IMB of Titan at $\sim 04.55 \text{ UTC}$, $|B| \approx 7 \text{ nT}$, $n_e \approx n_i \approx 0.1 \text{ cm}^{-3}$, the Alfvén speed $V_A = |B|/\sqrt{\mu_0 \rho} \approx 482 \text{ km}\cdot\text{s}^{-1}$. The bulk plasma velocity vector assumed ideal $\mathbf{V} = 90 \cdot [1 \ 0 \ 0] \text{ km}\cdot\text{s}^{-1}$.

To estimate the Doppler shift term $\mathbf{k} \cdot \mathbf{V}/2\pi = |k||V| \cos \theta_{kV}/2\pi$, the wave number must be estimated. Assuming the Alfvén wave dispersion relation, the wave number is $|k|/2\pi = f_{obs}/(V_A - |V| \cos \theta_{kV})$, and the Doppler shift

Table 1

The Wave Packet's Properties Are Calculated From the Minimum Variance Analysis Method for 0.016 Hz <math>f < 0.029</math> Hz Frequency Range

Number	Time interval, UTC	λ_1/λ_2	λ_2/λ_3	$\pm \mathbf{k}$	θ_{kB} [deg]	θ_{kV} [deg]	f'/f_{ci}
1	04:53:01–04:54:11	6.4	5.4	[1, −0.04, 0.01]	68	2 (178)	−0.05 (0.03)
2	04:53:59–04:55:47	2.8	23	[−0.89, −0.45, −0.07]	97	27 (153)	0.04 (−0.03)
3	04:57:36–04:58:54	4	5.3	[−0.6, −0.41, −0.72]	74	126 (54)	−0.02 (0.03)

Note. For each of the enumerated time intervals (columns 1 and 2), the ratio between maximum and intermediate λ_1/λ_2 (column 3), intermediate and minimum λ_2/λ_3 (column 4) eigenvalues of a variance matrix are calculated. In column 5 the estimated wave vector \mathbf{k} as the minimum variance direction is provided, as well as the angle θ_{kB} between the background magnetic field and the wave vector. Notice, that the wave vector has an uncertainty in sign. In columns 6 and 7, the angle between the wave vector and magnetic field θ_{kB} and the bulk velocity vector θ_{kV} is shown. Finally, in column 8 the normalized Doppler shift term contribution is shown, normalized to proton cyclotron frequency. The visual results of MVA can be found in Appendix A.

term $f_{ds} = f_{obs}|V|\cos\theta_{kV}/(V_A - |V|\cos\theta_{kV}) = f_{obs}M_A \cos\theta_{kV}/(1 - M_A \cos\theta_{kV})$. We applied MVA to estimate the wave vector in a range of frequencies 0.033 Hz <math>f < 0.081</math> Hz. We selected three wave packets for which the MVA shows the best result and calculated the corresponding normalized to the local proton cyclotron frequency Doppler shift frequency. From the last column of Table 1 it is clearly seen that one can neglect the Doppler shift term within a chosen frequency range.

3.6. The Pitch-Angle Modulation

Figure 7 shows an overview of pitch-angle distribution (PAD) at different energy ranges. The colorscale shows DEF normalized to the bin size of the PAD and the number of data points. The modulation of the PAD can be seen at the same time interval with enhanced wave activity and a broad spread of the electron energy distribution. The bin size is chosen so the data gaps are less than 20°. In the top panel (a) the instantaneous pitch-angle is calculated for each of eight CAPS/ELS anodes. In each panel, several electron populations are identified, however, it is not clear how these electron populations are related to the aforementioned electron observations in Section 3.4. The first obvious population can be seen until 04:52 UTC and is an ionospheric plasma or population (1) with an isotropic distribution. From around 04:52 UTC to 04:56 UTC in the energy channel $E < 13.9$ eV shown in panel (d) the enhancement in the DEF is seen. This enhancement is most likely connected to the accelerated ionospheric electrons, that is, population (2). In the energy ranges above 13.9 eV, the enhancement in DEF is also visible, but is less pronounced.

4. Discussion

4.1. Summary of the Observations and Interpretation

This paper investigated the Cassini T36 flyby to gain a deeper understanding of the structure and processes in the vicinity of Titan's induced magnetosphere. The flyby occurred when Titan was in Saturn's dayside magnetosphere at a Saturn local time ~ 12 hours, that is, noon sector. The focus of the paper is on the outbound leg, where quasi-periodic plasma structures were observed during the crossing of the MPR, in the time interval from 04.50 UTC to 05.00 UTC. Inside the MPR, low-frequency waves, below the proton cyclotron frequency ($f_{pc} \approx 0.1$ Hz), were observed together with dispersive plasma structures, appearing in the data as a rising tone with ~ 20 s period or a frequency of ≈ 0.05 Hz. It was also shown that the power of transverse fluctuations of the magnetic field B_{\perp} is larger than compressional B_{\parallel} at almost all frequencies. There are also localized peaks in the power spectral density that can correspond to the cyclotron frequencies of H^+ , H_2^+ , and O^+ . At the same time, the pitch-angle distribution was modulated with the same frequency as the energy distribution, with the most pronounced modulation in the energy range from about 13.9 eV up to several hundred eV. In addition to the above, the pitch-angle distribution across the whole energy range was not consistent with a loss-cone distribution, typical for trapped electrons, but rather similar to isotropic electrons. The spacecraft potential was modulated with the same frequency as the time-dependent dispersive electron structures. The most visible modulation was seen in anodes 3–5, indicating that the modulated electrons are dense and have an ionospheric origin, as these anodes are along the ram direction. Interestingly, the change in the spacecraft potential is less visible in other anodes—the same anodes, where the

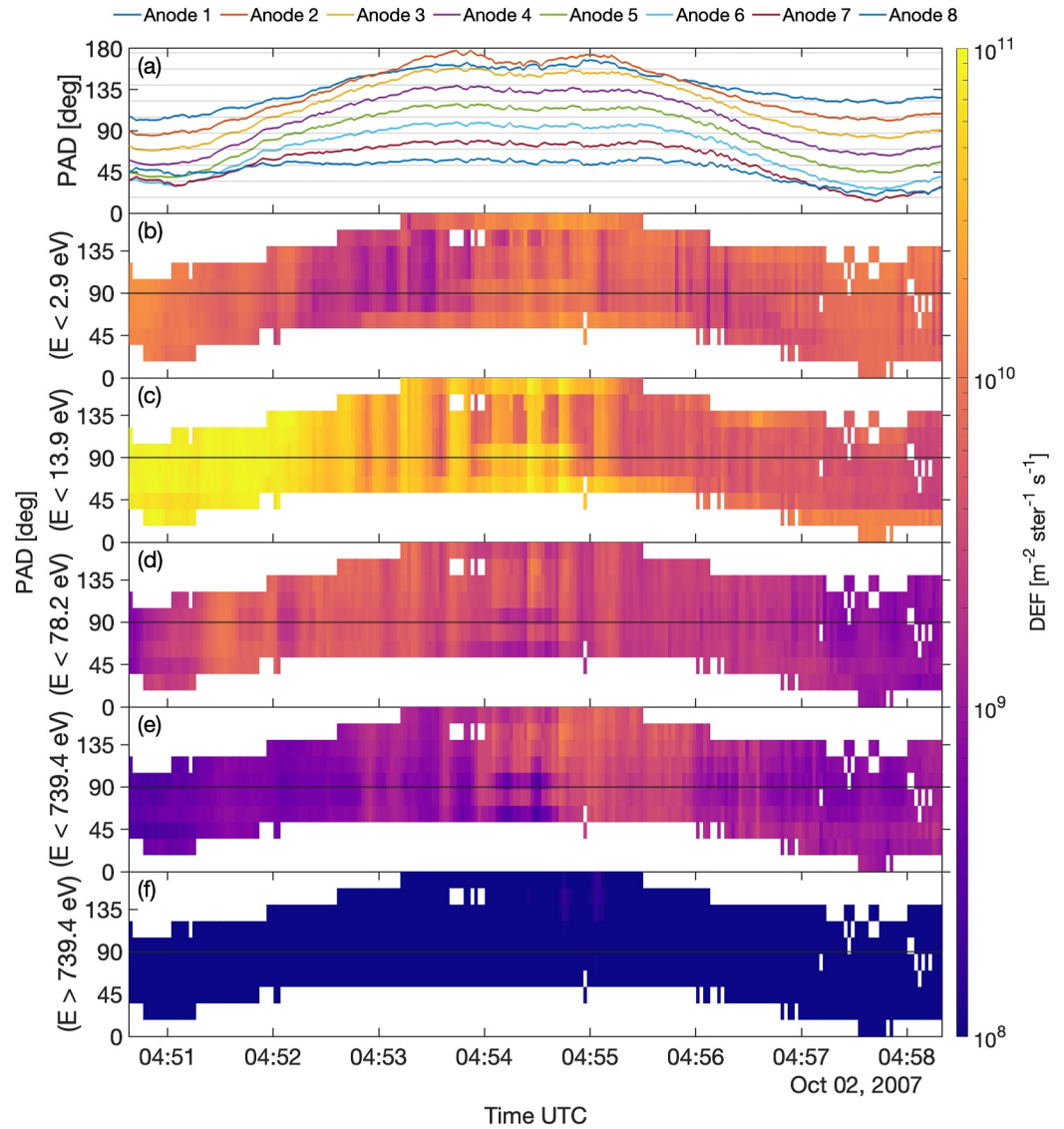


Figure 7. The overview of a pitch-angle distribution (PAD) made by using CAPS/ELS and divided into several energy ranges: (a) the instantaneous pitch-angle for each of the anodes, (b–f) the pitch-angle distribution for separate energy ranges, excluding the previous range.

low energy blob of electrons was observed. This is probably due to the overlap of the blob electron energy distribution with photoelectrons. The analysis of the upstream magnetic field direction suggests that Titan was in Saturn's magnetodisk plasma sheet throughout the whole duration of the flyby. In addition, the position of Saturn's magnetopause in proximity to Titan, suggests that Saturn's magnetosphere was compressed due to the increased solar wind dynamic pressure.

We have also considered but ruled out the disturbances in the local plasma environment induced by the spacecraft itself. According to the listed trajectory correction maneuvers using the main engine burns and thrusters firings, Magnetospheric Imaging Instrument (MIMI) discharge events, and RPWS sounder firings, none of them happened near the event time during the T36 flyby. The actuation period of the CAPS ELS does not impact the observations either, as an actuation period ($\approx 2\pi$ every 3 min) is longer than the observed periodicity of the observed plasma structures.

4.2. Possible Explanations

The observed plasma structures presented in this paper, manifested as modulated electron distribution and pick-up ions, have not been reported before and here we investigate possible driving mechanisms for their development. We propose that the observation is consistent with the ionospheric plasma outflow followed by the acceleration and formation of pick-up ions by the motional electric field. The modulation of an outflowing ionospheric plasma can be caused by higher-order electric fields. The low-frequency wave activity was thus due to the presence of dense and cold plasma, forming blobs and pick-up ions exciting low-amplitude alfvénic fluctuations, for example, ion-cyclotron or mirror mode waves. However, the source of the plasma injection periodicity remains unknown. It can be originated from a spatially or temporarily periodic source. It is also seen in Figure 1d, Saturn's magnetopause was located in the vicinity of Titan. The proximity of the MP to Titan indicates that Saturn's magnetosphere was compressed due to the increased upstream solar wind pressure. Despite pushing the magnetopause to Titan's orbit, there is no evidence that Titan was exposed to Saturn's magnetosheath plasma, neither in the ion and electron spectrogram (no signatures of H⁺ and He²⁺ ions, and thermalized solar wind electrons) nor magnetic field measurements, that is, magnetic field in the magnetosheath is ≈2 nT, no evidence of turbulent fields (e.g., Hadid et al., 2015).

The discussed escape process is non-thermal, the ionospheric plasma must be pulled out from the ionosphere with an electric field. The electric field in collisionless plasma of the IMB region at an altitude ≈1 – 1.5 R_T (resistivity is η = 0, thus the collisional ohmic term is ηJ = 0) is given by Ohm's law (neglecting the electron inertia term):

$$\mathbf{E} = \underbrace{-\mathbf{v} \times \mathbf{B}}_{\text{convective (1)}} + \underbrace{\frac{\mathbf{J} \times \mathbf{B}}{ne}}_{\text{Hall (2)}} - \underbrace{\frac{\nabla P_e}{ne}}_{\text{ambipolar (3)}}. \quad (1)$$

Depending on the scale of a process, each term of Equation 1 is responsible for different physics. For example, on the scales of ion inertial lengths $d_i = c/\omega_{pi}$, the Hall (2) term is responsible for ion acceleration. The Hall term results from the difference in motion between ions and electrons, while ions are demagnetized, electrons are frozen-in and carry out the magnetic field flux. The Hall electric field can be important in a region of draped magnetic field, for example, magnetotail and induced magnetosphere. The electron pressure or ambipolar term (3) allows electrons to decouple from the background magnetic field due to the electron pressure P_e . This term is important in the ionosphere, where electron density gradients exist and electrons are more mobile than ions, leading to an ambipolar electric field. The terms (2–3) in Equation 1 are called non-ideal, and these terms might contribute to a non-ideal, localized electric field, pulling out ionospheric plasma. Comparing the convective, Hall, and pressure terms in the induced magnetosphere region

$$\frac{|\mathbf{v} \times \mathbf{B}|}{|\nabla P_e/ne|} \sim \frac{v_c B}{n_e k_B T_e / (L_{P_e} n_e e)} \approx 10^2, \quad (2)$$

$$\frac{|\mathbf{v} \times \mathbf{B}|}{|\mathbf{J} \times \mathbf{B}/ne|} \sim \frac{v_c B}{B^2/\mu_0 / (L_{J \times B} n_e e)} \approx 10^1, \quad (3)$$

$$\frac{|\mathbf{J} \times \mathbf{B}|}{|\nabla P_e|} \sim \frac{B^2/\mu_0 / L_{J \times B}}{n_e k_B T_e / L_{P_e}} \approx 10^1, \quad (4)$$

where L_{P_e} and $L_{J \times B}$ are the characteristic scale of spatial variations of pressure gradient and Hall terms. We assume, that the flow velocity $v_c \approx 120 \text{ km s}^{-1}$, magnetic field is $|B| \approx 10 \text{ nT}$, electron density $n_e \approx 5 \text{ cm}^{-3}$ and electron temperature $T_e \approx 10^{-1} \text{ eV}$. We also assume that the characteristic scale of the magnetic field gradient $L_{J \times B} \approx R_T$, and the pressure gradient scale $L_{P_e} \approx 15 - 50 \text{ km}$ (about the scale height). The values in Equations 2–4 indicate that the convective electric field in the IMB has a greater impact on the large-scale ionospheric plasma acceleration. The Hall electric field is of second-order importance compared to the convective electric field and can result in localized plasma structures. The electron pressure gradient-driven electric field can be neglected. This is consistent with the analysis done by Romanelli et al. (2014), who addressed the influence of magnetic tension forces in Titan's induced magnetotail. A similar conclusion was found by Boscoboinik

et al. (2023) by analyzing the forces and fields in the multi-fluid MHD simulation at Mars. It was also found that the scale of the interaction region is particularly important for the Hall term as it scales as an ion inertial length.

We now check two mechanisms for producing non-ideal electric fields. A shear instability is a way to set up an electric field by separating ions and electrons across the boundary layer. If a shear flow in the vicinity of an induced magnetosphere boundary is significant, then the boundary can be unstable to Kelvin-Helmholtz instability (KHI). The dispersion relation for a KHI depends on plasma parameters on both sides of the boundary (e.g., Treumann & Baumjohann, 1997)

$$(\mathbf{k} \cdot \mathbf{v}_0)^2 > \frac{n_1 + n_2}{n_1 n_2} [n_1 (\mathbf{k} \cdot \mathbf{v}_{A1})^2 + n_2 (\mathbf{k} \cdot \mathbf{v}_{A2})^2], \quad (5)$$

where \mathbf{v}_0 is a bulk flow velocity, \mathbf{v}_{A1} and \mathbf{v}_{A2} Alfvén velocity, n_1 and n_2 plasma density on both sides of a boundary. The threshold is the lowest when the magnetic field is perpendicular to the wave propagation (the right-hand side of Equation 5 is zero). For observed averaged magnetospheric ($n_1 \approx 10^{-1} \text{ cm}^{-3}$, $|B| \approx 7 \text{ nT}$, $v_{A1} \approx 483 \text{ km s}^{-1}$) and ionospheric ($n_2 \approx 10^2 \text{ cm}^{-3}$, $|B| \approx 10 \text{ nT}$, $v_{A2} \approx 22 \text{ km s}^{-1}$) parameters, assuming quasi-neutrality $n_e \sim n_i \sim n$, $\mathbf{k} \perp \mathbf{B}$ and ideal corotation $\mathbf{k} \perp \mathbf{v}_0$, the upstream bulk velocity is estimated as $v_0 \approx 847 \text{ km s}^{-1}$, which is $\sim 7\text{--}9$ times larger than the ideal corotational velocity $90\text{--}120 \text{ km s}^{-1}$. Therefore it is unlikely that the shearing instability plays any significant role.

One can also argue that the observed electron distribution time dispersion is due to the transfer of energy from the observed low-frequency waves. The problem with this type of wave-particle interaction is that low-frequency waves transmit energy to ions, causing heating, whereas electrons are too mobile and unaffected by MHD modes. In the provided observations electrons gain energy from a few eV to several hundreds of eV over roughly 20 s, thus the electron energy gain rate $\epsilon_e \approx 10 \text{ eV s}^{-1}$. The wave energy is proportional to the amplitude of the wave. From the observations, the maximum amplitude of the magnetic field fluctuations $\delta B_{\text{max}} \approx 1 \text{ nT}$, therefore the corresponding magnetic energy density is $W_B = \delta B_{\text{max}}^2 / 2\mu_0 \approx 2.5 \text{ eV cm}^{-3}$, where μ_0 is a magnetic permeability. The flux of energy is thus $\Phi = V_A W_B$, and the energy transfer rate per electron is thus $\epsilon = \Phi / n_e l = V_A W_B / n_e l$, where l is the size of the interaction region, and V_A the Alfvén speed of a wave. Assuming that all the energy is transferred from the wave to electrons, density $n_e \approx 0.1 \text{ cm}^{-3}$, the magnetic field amplitude $\delta B = 0.1 - 1 \text{ nT}$, the size of the interaction region is $l = v_{sc} \cdot 20 \text{ s}$ ($v_{sc} \approx 6 \text{ km s}^{-1}$, 20 s period of an electron energization), and the ion component consists only of protons, the energy transfer rate $\epsilon_B = 10^{-1} - 10^1 \text{ eV s}^{-1}$. The rate at which the wave under the following assumptions can transfer energy to electrons $\epsilon_b \leq \epsilon_e$. However, the reader should be careful since the calculations are based on the order of magnitude analysis, and many parameters are averaged. In addition, the MHD nature of the observed magnetic fluctuations should be taken into account for such a type of analysis, namely, the magnetic field energy is converted mostly into ion heating/energization $\epsilon_i \approx \epsilon_B$. Thus the conclusion is, that at least the ion heating/energization rate ϵ_i is somewhat comparable to the electron energy gain rate ϵ_e . The thorough analysis of the energy transfer is beyond the scope of this paper but can be conducted once the kinetic parameters of plasma (e.g., 3D electron distribution function) and waves (e.g., wave mode, phase speed) are defined.

Another explanation would be to connect the observed plasma structures to mirror mode structures or low-frequency waves. The mirror mode is a non-propagating in the plasma rest frame, linearly polarized, zero-frequency wave (only damping or growth are allowed), appearing in data as anti-correlated dips and peaks of the magnetic field and plasma density (e.g., Hasegawa, 1969). As the mirror mode wave has similar to the magnetic bottle topology, electrons and ions can be trapped inside the structure, therefore the pitch-angle distribution should follow the critical angle $\alpha = \sin^{-1} B/B_{bg}$. For the mirror instability to grow, a significant pressure anisotropy in high- β plasmas has to be developed, and the instability threshold is yielded by the plasma beta $\beta = nk_B T / (B^2 / 2\mu_0)$ or $\beta_{\perp} / \beta_{\parallel} > 1 + 1/\beta_{\perp}$ (e.g., Hasegawa, 1969). The perpendicular pressure can grow due to heating processes observed downstream of bow shocks, however, when Titan is submerged into the submagnetosonic magnetospheric flow of Saturn, the bow shock is not formed and Titan lacks such a heating mechanism. In addition, it is impossible to estimate reasonably the parallel and perpendicular components of the pressure tensor, as the pitch-angle coverage is not full. The presence of pick-up ions indicates that the temperature anisotropy is present (as pick-up ions have a ring-beam distribution at the moment of injection) (e.g., Ledvina et al., 2005), but not strong enough to either exceed the mirror instability threshold or the growth rate is too slow.

As mentioned before, the proximity of Saturn's dayside magnetopause to Titan's orbit indicates an increased upstream solar wind pressure. The magnetopause can respond to such variations in the upstream pressure by the compression of the magnetosphere and generation of ultra-low frequency (ULF) waves propagating inward, into the magnetosphere of Saturn and across the magnetopause, similar to Earth (e.g., Desai et al., 2021; Freeman et al., 1995). The ULF waves are electromagnetic low-frequency waves, below the ion-cyclotron frequency, and play a significant role in the energy and momentum transfer across the magnetopause. It was shown that the magnetopause surface waves when propagating tailward could be amplified through the Kelvin-Helmholtz instability (e.g., Archer et al., 2021). The combined observations of XMM-Newton and Juno of the x-ray aurora at Jupiter by Yao et al. (2021) showed that ULF waves can modulate electromagnetic ion-cyclotron waves, and consequently modulate the ion precipitation in Jupiter's auroral region. If extrapolating to the current case, Saturn's magnetopause could generate ULF waves as a response to an increased solar wind pressure. The propagated ULF waves thus may interact with Titan's induced magnetosphere and a region of active pick-up ion generation, causing the quasi-periodic modulation of the ion and electron distribution and low-frequency waves.

Worth mentioning is the hybrid simulation by Ledvina et al. (2012), which reproduces some of the observed features. In the simulation, Ledvina et al. (2012) addressed how the orientation of the dayside ionosphere with respect to the incident magnetospheric plasma flow affects the escape rate and electric and magnetic fields. In one of the cases, when the orientation of the dayside ionosphere is similar to the T36 flyby, the outflowing plasma blobs on the anti-Saturn side of the ionosphere cause electromagnetic waves and turbulence to emerge. The plasma blobs were associated with the pick-up ions and originated from the upstream of Titan. The plasma blobs are then convected to the flank IMB perturbing the electromagnetic fields and producing turbulence. It is consistent with the features we observed during the T36 flyby: the plasma structures are found in the flank IMB region, the periodicity is on a similar scale as the ion-cyclotron frequency, and there is a low frequency and amplitude wave activity. As the simulation was also steady-state, the similarities can be explained by the non-time-varying upstream conditions.

4.3. Limitation of the Analysis and Similar Observations

The detection of the observed plasma structures unveils the complexity of Titan's induced magnetosphere and the diversity of plasma processes in this region. It is important because it affects the non-thermal plasma escape. The mechanism behind the quasi-periodic modulation remains unknown. The explanation is most likely connected to spatial and temporal variability in Titan's ionosphere. A temporal variation of Titan's ionosphere on the scale of ion cyclotron frequency is not reported in the literature. The spatial irregularities in Titan's ionosphere might be connected to a dayside-nightside asymmetry in the production rate of electrons, non-uniform distribution of the background energetic particles, and generation of pick-up ions. We also do not know how the electrons are pulled out of the ionosphere, or what is the exact mechanism of the electron energization.

The limitations of the interpretation are imposed by the instrument's field of view and the low time resolution of both ion and electron moments. The actuation of the field of view at 1° per second rate takes 180 s to cover the entire field-of-view hemisphere and does not allow resolving the full instantaneous energy-mass-, and pitch-angle distribution. The ion distribution measurements are more affected by the field-of-view limitations which limit to a certain extent the calculations of plasma moments, and also suffer from the lack of 3D distribution measurements. It takes 4 s for ions and 2 s for electrons to sweep through the full energy range, which is a reasonable time resolution when focusing on slow processes. The low time resolution of plasma moments does not allow for full interpretation of the observations, for example, the anti-correlation of the magnetic field with the electron density will indicate the presence of the mirror mode or slow magnetosonic waves. The absence of particular wave modes might indicate that the measurements were made outside of the active source region of waves. The low-frequency and low-resolution measurements of the electric field and magnetic field are also contaminated by the spacecraft-induced noise, for example, high-gain antenna perturbs the search-coil magnetometers. The possible role of waves must be investigated as well as their impact on electron energization and scattering, and the effect of waves on a local structure of the induced magnetosphere. The presence of alfvénic fluctuations itself is a rare event. For example, ion cyclotron waves were detected during the T63 and T98 flybys by Russell et al. (2016). These plasma waves are hard to observe as argued by Cowee et al. (2010) due to a longer wave growth time compared with the ambient plasma convection time, meaning there is not enough time for a wave to grow to large amplitudes.

The effective mechanisms of plasma heating, for example, the bow shock, are absent at Titan. The alfvénic resonator properties of Titan ionosphere, such as absorption or reflection of Alfvén waves by the ionosphere, under particular circumstances, are highly dependent on the magnetic field strength (e.g., Rosenqvist et al., 2009). Another interesting possibility is a conversion of the Alfvén waves into dispersive Alfvén waves (DAW) (e.g., Stasiewicz et al., 2000) due to the increase of a perpendicular wavelength up to ion gyroradius. The DAW can accelerate electrons into Titan's ionosphere as they carry on the parallel electric field and produce dispersive signatures.

Similar plasma structures were observed at Mars (e.g., Bertucci et al., 2004; Halekas et al., 2016; Ruhunusiri et al., 2016). In Bertucci et al. (2004) the low-frequency waves and magnetic pile-up in the martian induced magnetosphere were studied. Using the Mars Global Surveyor data it was shown that in the magnetic pile-up region, the mirror mode waves were detected. The temperature anisotropy is provided by the bow shock, satisfying the mirror instability threshold. These structures are then convected downstream of the shock and piled in the IMB. Based on observations by the Mars Atmosphere and Volatile Evolution mission (MAVEN), Halekas et al. (2016) reported on plasma blobs similar to the one observed by Cassini during the T36 flyby. However, despite similarities in plasma signatures, the magnetic field signatures are not consistent with the T36 flyby. In Ruhunusiri et al. (2016) the partially developed vortexes of Kelvin-Helmholtz instability were observed in the martian induced magnetosphere. The vortexes are a result of the sheath and ionospheric plasma mixing in the induced magnetosphere boundary due to a velocity shear across the boundary. Similar to boundary oscillation, the magnetic field signatures are also not consistent with the T36 flyby. One would expect to observe intermittent crossings of the boundary with the change in the magnetic topology.

What can be done to address the generation mechanism of the observed structures? Since Cassini has not been operative since 2017 and no further mission with a plasma and fields suite has been confirmed/announced, we speculate what kind of measurements can be done. It is rather rare for a planetary mission to have multi-spacecraft measurements, therefore we also focus on single-spacecraft observations. From the point of view of plasma measurements, the high-resolution 3D ion and electron distribution function measurements in the IMB would help to quantify better plasma properties, that is, density, velocity, and temperature, of Titan's induced magnetosphere. The low-frequency magnetic and electric field measurements would also play an important role in characterizing the electromagnetic environment, that is, wave properties, and wave-particle interactions. In the meantime, plasma simulation efforts can also be made. Since the nature of the observed plasma structures seems to be modulated on ion scales, the multi-species hybrid-Vlasov simulation with a focus on the induced magnetosphere region would be of interest. From the simulation, one can estimate the relative contribution of various terms in the generalized Ohm's law to the dynamics of plasma in the IMB. However, the problem with this simulation setup is that electron dynamics cannot be captured accurately by hybrid simulations, but rather by particle-in-cell type simulations. The solution is to artificially reduce the proton-to-electron mass ratio to speed up the simulation. With that, it is possible to track simultaneously both ion and electron physics in the same region.

5. Conclusions

In this paper, the properties of a set of unique electron plasma structures are characterized using the plasma and magnetic field measurements of Cassini during the T36 flyby. We observed a complex structure of Titan's induced magnetosphere consisting of at least four electron populations and possessing low-frequency wave activity. The observed plasma structures appear as modulated accelerated ionospheric electrons with a modulation period of ~ 20 seconds, which is at about the local proton cyclotron frequency. The low-frequency wave burst (below the proton cyclotron frequency), predominantly transverse, was seen within the same region. The pitch-angle distribution is modulated in the same fashion as the energy distribution. The exact modulation mechanism is unknown, but we rule out that the observed plasma structures could not result from a shearing instability, that is, Kelvin-Helmholtz instability. We estimate that the pulling of plasma from the ionosphere due to $\mathbf{J} \times \mathbf{B}$ forces play a more significant role than the pressure gradient ∇P_e . We also highlight the importance of Titan's proximity to Saturn's dayside magnetopause, as it indicates that Saturn's magnetosphere experienced an increase in the upstream solar wind pressure leading to the compression of Saturn's magnetosphere.

The T36 flyby is of interest when trying to understand the moon-plasma interaction and, in particular, Titan science for several reasons. First of all, it highlights the complexity of Titan's plasma environment, which is

subject to multiple sources of modulations, for example, seasonal and rotational (due to Saturn's rapid rotation). This observation provides another source of modulation on the ion scale, the origin of which can be investigated in the future. Secondly, the presence of low-frequency magnetic field fluctuations gives us a hint of the possible contribution of plasma waves on the local structure and processes in Titan's induced magnetosphere. The correlation analysis between the observed quasi-periodic plasma structures and low-frequency wave activity is limited due to the instrumentation flaws and can be improved in future missions or by high-resolution hybrid or particle-in-cell simulations.

Appendix A: Minimum Variance Analysis (MVA) Results

The results of the MVA analysis are shown in Figures A1–A3. The MVA was performed for the time intervals presented in Table 1. The top panel (a) shows the three components of the measured magnetic field in THS, the next panel (b) shows the three components of the magnetic field in the LMN reference frame (corresponding to

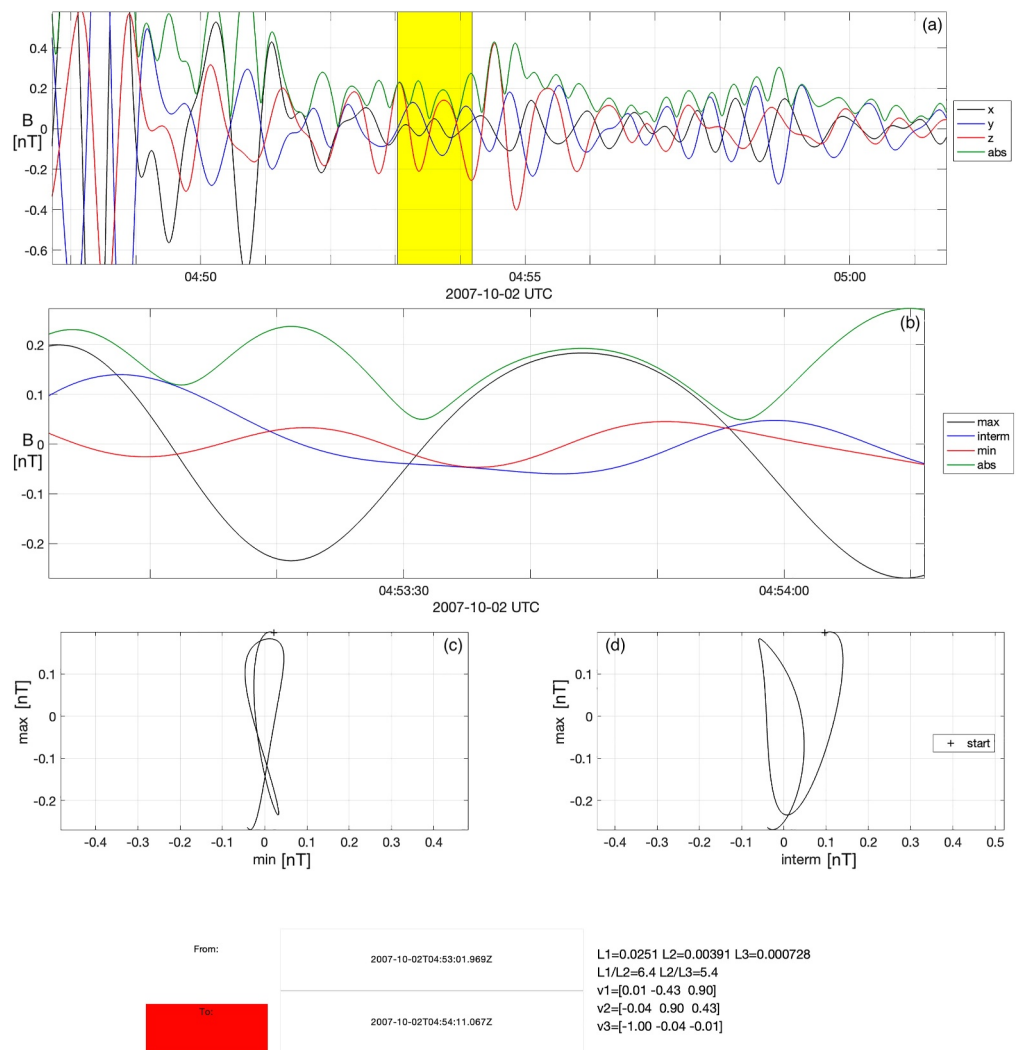


Figure A1. The results of the minimum variance analysis (MVA) applied to the first time interval in Table 1: (a) three components of the magnetic field in THS frame, (b) three components of the magnetic field in LMN (maximum, intermediate, minimum), (c) and (d) projections of the magnetic field hodogram in LN (maximum-minimum) and LM (maximum-intermediate) planes.

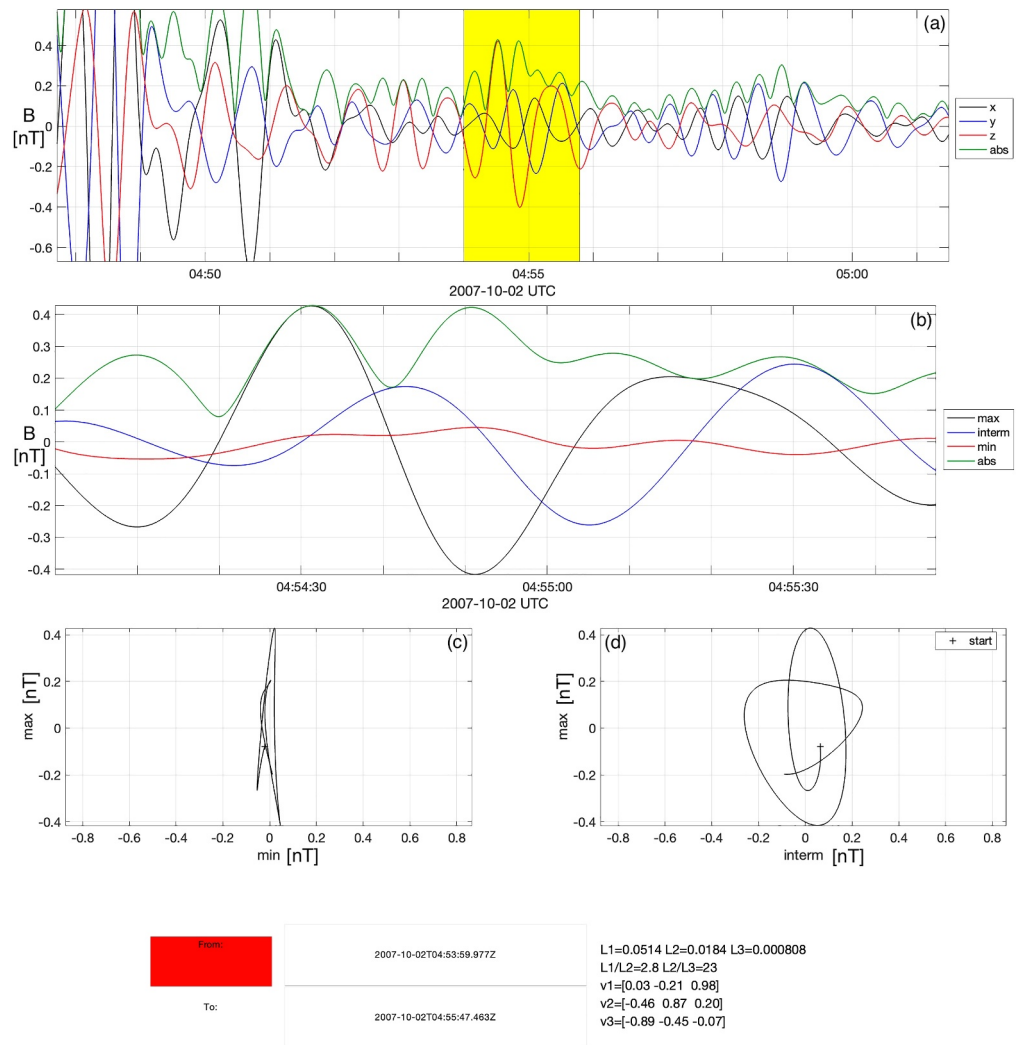


Figure A2. The results of the minimum variance analysis (MVA) applied to the second time interval in Table 1.

the maximum, intermediate and minimum variance axes). The bottom panels (c) and (d) show the hodogram of the magnetic field in the LN (maximum-minimum) and LM (maximum-intermediate) projections.

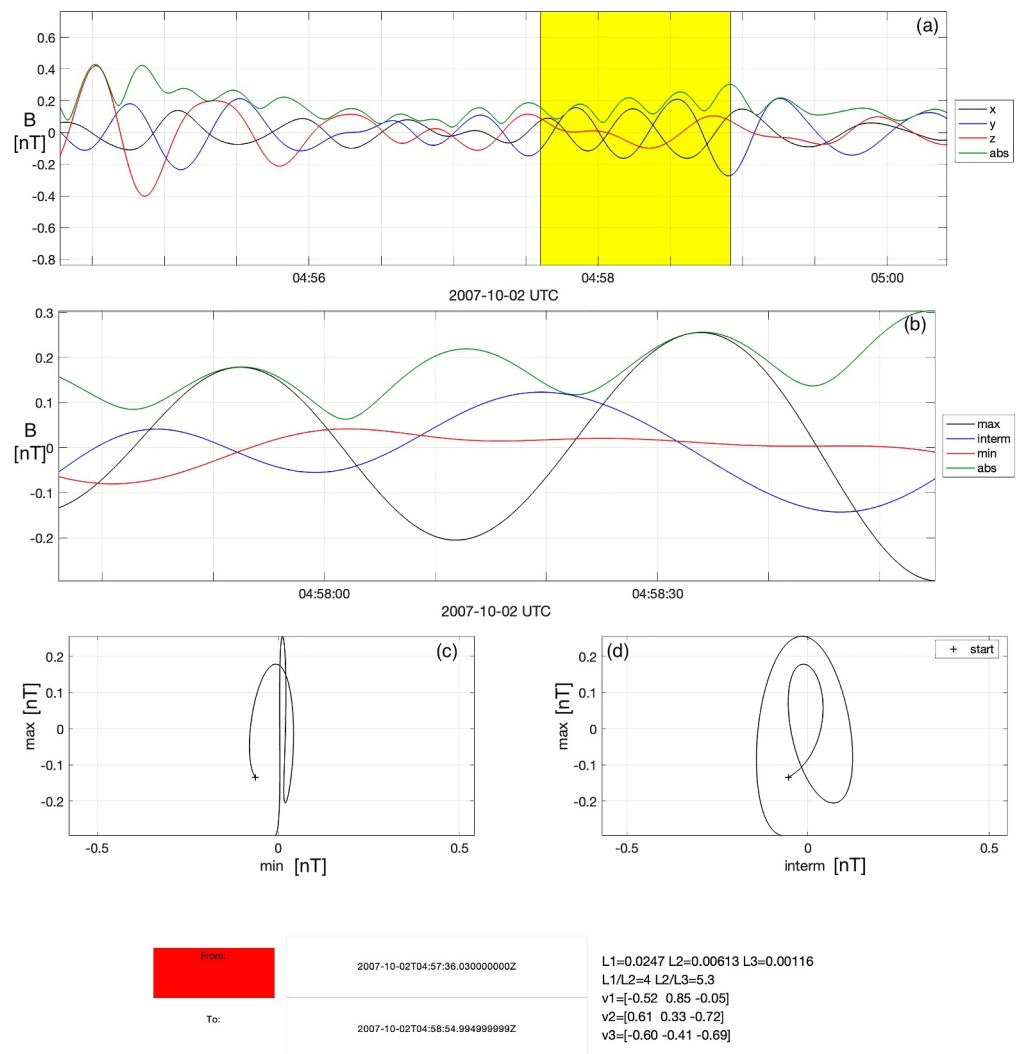


Figure A3. The results of the minimum variance analysis (MVA) applied to the third time interval in Table 1.

Data Availability Statement

For the wavelet transform we used MATLAB-based library irfu-matlab (Khotyaintsev et al., 2024). The RPWS wave and upper-hybrid electron density data was provided by Gurnett et al. (2020). The magnetic field measurements were provided by M. Dougherty et al. (2023). The electron and ion spectrometer CAPS ELS and IMS data was provided by Waite and Wilson (2022). The electron density and temperature, and spacecraft potential from the RPWS Langmuir probe sweeps were taken from <https://pds-ppi.igpp.ucla.edu/data/CO-SS-RPWS-5-LPSWEEP-V1.0/>. The list of the spacecraft perturbations https://atmos.nmsu.edu/data_and_services/atmospheres_data/Cassini/eng-overview.html#noise. The data sets to reproduce the figures can be found here Kim and Edberg (2025).

Acknowledgments

KK and NE acknowledge funding from the Swedish Research Council (Vetenskapsrådet) under contract 2020-03962. AW and AJC acknowledge partial support from STFC Grants ST/S000240/1 and ST/W001004/1. The authors are also grateful to SNSA (formerly SNSB) who supported the RPWS/LP instrument onboard Cassini. The reader can also refer to the following data sets from Kim and Edberg (2025).

References

- Ågren, K., Wahlund, J.-E., Garnier, P., Modolo, R., Cui, J., Galand, M., & Müller-Wodarg, I. (2009). On the ionospheric structure of Titan. *Planetary and Space Science*, 57(14), 1821–1827. <https://doi.org/10.1016/j.pss.2009.04.012>
- Archer, M. O., Hartinger, M. D., Plaschke, F., Southwood, D. J., & Rastaetter, L. (2021). Magnetopause ripples going against the flow form azimuthally stationary surface waves. *Nature Communications*, 12(1), 5697. <https://doi.org/10.1038/s41467-021-25923-7>
- Arridge, C. S., André, N., Bertucci, C. L., Garnier, P., Jackman, C. M., Németh, Z., et al. (2011). Upstream of Saturn and Titan. *Space Science Reviews*, 162(1–4), 25–83. <https://doi.org/10.1007/s11214-011-9849-x>
- Backes, H., Neubauer, F. M., Dougherty, M. K., Achilleos, N., André, N., Arridge, C. S., et al. (2005). Titan's magnetic field signature during the first Cassini encounter. *Science*, 308(5724), 992–995. <https://doi.org/10.1126/science.1109763>

- Bertucci, C., Achilleos, N., Dougherty, M. K., Modolo, R., Coates, A. J., Szego, K., et al. (2008). The magnetic memory of Titan's ionized atmosphere. *Science*, 321(5895), 1475–1478. <https://doi.org/10.1126/science.1159780>
- Bertucci, C., Hamilton, D. C., Kurth, W. S., Hospodarsky, G., Mitchell, D., Sergis, N., et al. (2015). Titan's interaction with the supersonic solar wind. *Geophysical Research Letters*, 42(2), 193–200. <https://doi.org/10.1002/2014GL062106>
- Bertucci, C., Mazelle, C., Crider, D. H., Mitchell, D. L., Sauer, K., Acuña, M. H., et al. (2004). MGS MAG/ER observations at the magnetic pileup boundary of Mars: Draping enhancement and low frequency waves. *Advances in Space Research*, 33(11), 1938–1944. <https://doi.org/10.1016/j.asr.2003.04.054>
- Boscoboinik, G., Bertucci, C., Gomez, D., Dong, C., Regoli, L., Mazelle, C., et al. (2023). Forces, electric fields and currents at the subsolar Martian MPB: MAVEN observations and multifluid MHD simulation. *Icarus*, 401, 115598. <https://doi.org/10.1016/j.icarus.2023.115598>
- Burne, S., Bertucci, C., Sergis, N., Morales, L. F., Achilleos, N., Sánchez-Cano, B., et al. (2023). Space weather in the Saturn-Titan system. *The Astrophysical Journal*, 948(1), 37. <https://doi.org/10.3847/1538-4357/acc738>
- Chatain, A., Wahlund, J. E., Shebanits, O., Hadid, L. Z., Morooka, M., Edberg, N. J. T., et al. (2021). Re-analysis of the Cassini RPWS/LP data in Titan's ionosphere: I. Detection of several electron populations. *Journal of Geophysical Research: Space Physics*, 126(8), e28412. <https://doi.org/10.1029/2020JA028412>
- Chen, C., & Simon, S. (2020). A comprehensive study of Titan's magnetic pile-up region during the Cassini era. *Planetary and Space Science*, 191, 105037. <https://doi.org/10.1016/j.pss.2020.105037>
- Coates, A. J., Crary, F. J., Lewis, G. R., Young, D. T., Waite, J. H., & Sittler, E. C. (2007). Discovery of heavy negative ions in Titan's ionosphere. *Geophysical Research Letters*, 34(22), L22103. <https://doi.org/10.1029/2007GL030978>
- Coates, A. J., Wellbrock, A., Waite, J. H., & Jones, G. H. (2015). A new upper limit to the field-aligned potential near Titan. *Geophysical Research Letters*, 42(12), 4676–4684. <https://doi.org/10.1002/2015GL064474>
- Cowee, M. M., Gary, S. P., Wei, H. Y., Tokar, R. L., & Russell, C. T. (2010). An explanation for the lack of ion cyclotron wave generation by pickup ions at Titan: 1-D hybrid simulation results. *Journal of Geophysical Research*, 115(A10), A10224. <https://doi.org/10.1029/2010JA015769>
- Desai, R. T., Coates, A. J., Wellbrock, A., Vuitton, V., Crary, F. J., González-Caniulef, D., et al. (2017). Carbon chain anions and the growth of complex organic molecules in Titan's ionosphere. *The Astrophysical Journal Letters*, 844(2), L18. <https://doi.org/10.3847/2041-8213/aa7851>
- Desai, R. T., Freeman, M. P., Eastwood, J. P., Eggington, J. W. B., Archer, M. O., Shprits, Y. Y., et al. (2021). Interplanetary shock-induced magnetopause motion: Comparison between theory and global magnetohydrodynamic simulations. *Geophysical Research Letters*, 48(16), e92554. <https://doi.org/10.1029/2021GL092554>
- Dóbe, Z., & Szegő, K. (2005). Wave activity above the ionosphere of Titan: Predictions for the Cassini mission. *Journal of Geophysical Research*, 110(A3), A03224. <https://doi.org/10.1029/2004JA010548>
- Dougherty, M., Kellock, S., Slootweg, A., Achilleos, N., Joy, S., & Mafi, J. (2023). Cassini MAG Calibrated Full Res. Data in KRTP Coords. Collection. NASA Planetary Data System. urn:nasa:pds:cassini-mag-cal:data-full-krtp:1.0. <https://doi.org/10.17189/7PDG-DA68>
- Dougherty, M. K., Kellock, S., Southwood, D. J., Balogh, A., Smith, E. J., Tsurutani, B. T., et al. (2004). The Cassini magnetic field investigation. *Space Science Reviews*, 114(1–4), 331–383. <https://doi.org/10.1007/s11214-004-1432-2>
- Edberg, N. J. T., Andrews, D. J., Shebanits, O., Ögren, K., Wahlund, J. E., Opgenoorth, H. J., et al. (2013). Extreme densities in Titan's ionosphere during the T85 magnetosheath encounter. *Geophysical Research Letters*, 40(12), 2879–2883. <https://doi.org/10.1002/grl.50579>
- Feyerabend, M., Simon, S., Neubauer, F. M., Motschmann, U., Bertucci, C., Edberg, N. J. T., et al. (2016). Hybrid simulation of Titan's interaction with the supersonic solar wind during Cassini's T96 flyby. *Geophysical Research Letters*, 43(1), 35–42. <https://doi.org/10.1002/2015GL066848>
- Freeman, M. P., Freeman, N. C., & Farrugia, C. J. (1995). A linear perturbation analysis of magnetopause motion in the Newton-Busemann limit. *Annales Geophysicae*, 13(9), 907–918. <https://doi.org/10.1007/s00585-995-0907-0>
- Gurnett, D. A., Kurth, W. S., Kirchner, D. L., Hospodarsky, G. B., Averkamp, T. F., Zarka, P., et al. (2004). The Cassini radio and plasma wave investigation. *Space Science Reviews*, 114(1–4), 395–463. <https://doi.org/10.1007/s11214-004-1434-0>
- Gurnett, D. A., Wahlund, J. E., Kurth, W. S., West, E. E., Groene, J. B., & Persoon, A. M. (2020). Cassini RPWS electron densities from upper hybrid and plasma wave frequencies. NASA Planetary Data System. urn:nasa:pds:cassini-rpws-electron_density:data:1.0. <https://doi.org/10.17189/1518302>
- Gustafsson, G., & Wahlund, J. E. (2010). Electron temperatures in Saturn's plasma disc. *Planetary and Space Science*, 58(7–8), 1018–1025. <https://doi.org/10.1016/j.pss.2010.03.007>
- Hadid, L. Z., Sahraoui, F., Kiyani, K. H., Retinò, A., Modolo, R., Canu, P., et al. (2015). Nature of the MHD and kinetic scale turbulence in the magnetosheath of Saturn: Cassini observations. *The Astrophysical Journal Letters*, 813(2), L29. <https://doi.org/10.1088/2041-8205/813/2/L29>
- Halekas, J. S., Brain, D. A., Ruhunusiri, S., McFadden, J. P., Mitchell, D. L., Mazelle, C., et al. (2016). Plasma clouds and snowplows: Bulk plasma escape from Mars observed by MAVEN. *Geophysical Research Letters*, 43(4), 1426–1434. <https://doi.org/10.1002/2016GL067752>
- Hartle, R. E., Sittler, E. C., Neubauer, F. M., Johnson, R. E., Smith, H. T., Crary, F., et al. (2006). Initial interpretation of Titan plasma interaction as observed by the Cassini plasma spectrometer: Comparisons with Voyager 1. *Planetary and Space Science*, 54(12), 1211–1224. <https://doi.org/10.1016/j.pss.2006.05.029>
- Hasegawa, A. (1969). Drift mirror instability of the magnetosphere. *Physics of Fluids*, 12, 2642–2650. <https://doi.org/10.1063/1.1692407>
- Kabanovic, S., Simon, S., Neubauer, F. M., & Meeks, Z. (2017). An empirical model of Titan's magnetic environment during the Cassini era: Evidence for seasonal variability. *Journal of Geophysical Research: Space Physics*, 122(11), 11076–11085. <https://doi.org/10.1002/2017JA024402>
- Kanani, S. J., Arridge, C. S., Jones, G. H., Fazakerley, A. N., McAndrews, H. J., Sergis, N., et al. (2010). A new form of Saturn's magnetopause using a dynamic pressure balance model, based on in situ, multi-instrument Cassini measurements. *Journal of Geophysical Research*, 115(A6), 2009JA014262. <https://doi.org/10.1029/2009JA014262>
- Khotyaintsev, Y., Nilsson, T., Johansson, E. P. G., Vaivads, A., Graham, D., Karlsson, J., et al. (2024). IRFU-Matlab. *Zenodo*. <https://doi.org/10.5281/zenodo.14525047>
- Kim, K., & Edberg, N. J. (2025). The supporting datasets for the 2024JE008802RR submission [Dataset]. *Zenodo*. <https://doi.org/10.5281/zenodo.15261614>
- Kim, K., Edberg, N. J. T., Shebanits, O., Wahlund, J.-E., Vigren, E., & Bertucci, C. (2023). On current sheets and associated density spikes in Titan's ionosphere as seen from Cassini. *Journal of Geophysical Research: Space Physics*, 128(3), e2022JA031118. <https://doi.org/10.1029/2022JA031118>
- Kivelson, M. G., & Russell, C. T. (1995). Introduction to space physics. <https://doi.org/10.1017/9781139878296>

- Knetter, T., Neubauer, F. M., Horbury, T., & Balogh, A. (2004). Four-point discontinuity observations using Cluster magnetic field data: A statistical survey. *Journal of Geophysical Research*, *109*(A6), A06102. <https://doi.org/10.1029/2003JA010099>
- Ledvina, S. A., Brecht, S. H., & Cravens, T. E. (2012). The orientation of Titan's dayside ionosphere and its effects on Titan's plasma interaction. *Earth Planets and Space*, *64*(2), 207–230. <https://doi.org/10.5047/eps.2011.08.009>
- Ledvina, S. A., Cravens, T. E., & KecskeMÉTy, K. (2005). Ion distributions in Saturn's magnetosphere near Titan. *Journal of Geophysical Research*, *110*(A6), A06211. <https://doi.org/10.1029/2004JA010771>
- Masters, A., Achilleos, N., Dougherty, M. K., Slavín, J. A., Hospodarsky, G. B., Arridge, C. S., & Coates, A. J. (2008). An empirical model of Saturn's bow shock: Cassini observations of shock location and shape. *Journal of Geophysical Research*, *113*(A10), 2008JA013276. <https://doi.org/10.1029/2008JA013276>
- Mihalescu, T., Desai, R. T., Shebanits, O., Haythornthwaite, R., Wellbrock, A., Coates, A. J., et al. (2020). Spatial variations of low-mass negative ions in Titan's upper atmosphere. *The Planetary Science Journal*, *1*(2), 50. <https://doi.org/10.3847/PSJ/abb1ba>
- Morooka, M. W., Wahlund, J. E., Eriksson, A. I., Farrell, W. M., Gurnett, D. A., Kurth, W. S., et al. (2011). Dusty plasma in the vicinity of Enceladus. *Journal of Geophysical Research*, *116*(A12), A12221. <https://doi.org/10.1029/2011JA017038>
- Ness, N. F., Acuna, M. H., Behannon, K. W., & Neubauer, F. M. (1982). The induced magnetosphere of Titan. *Journal of Geophysical Research*, *87*(A3), 1369–1382. <https://doi.org/10.1029/JA087iA03p01369>
- Omidí, N., Sulaiman, A. H., Kurth, W., Madanian, H., Cravens, T., Sergis, N., et al. (2017). A single deformed bow shock for Titan-Saturn system. *Journal of Geophysical Research: Space Physics*, *122*(11), 11058–11075. <https://doi.org/10.1002/2017JA024672>
- Regoli, L. H., Coates, A. J., Thomsen, M. F., Jones, G. H., Roussos, E., Waite, J. H., et al. (2016). Survey of pickup ion signatures in the vicinity of Titan using CAPS/IMS. *Journal of Geophysical Research: Space Physics*, *121*(9), 8317–8328. <https://doi.org/10.1002/2016JA022617>
- Romanelli, N., Modolo, R., Dubinin, E., Berthelier, J. J., Bertucci, C., Wahlund, J. E., et al. (2014). Outflow and plasma acceleration in Titan's induced magnetotail: Evidence of magnetic tension forces. *Journal of Geophysical Research: Space Physics*, *119*(12), 9992–10005. <https://doi.org/10.1002/2014JA020391>
- Rosenqvist, L., Wahlund, J. E., Ågren, K., Modolo, R., Opgenoorth, H. J., Strobel, D., et al. (2009). Titan ionospheric conductivities from Cassini measurements. *Planetary and Space Science*, *57*(14–15), 1828–1833. <https://doi.org/10.1016/j.pss.2009.01.007>
- Ruhunusiri, S., Halekas, J. S., McFadden, J. P., Connerney, J. E. P., Espley, J. R., Harada, Y., et al. (2016). MAVEN observations of partially developed Kelvin-Helmholtz vortices at Mars. *Geophysical Research Letters*, *43*(10), 4763–4773. <https://doi.org/10.1002/2016GL068926>
- Russell, C. T., Wei, H. Y., Cowee, M. M., Neubauer, F. M., & Dougherty, M. K. (2016). Ion cyclotron waves at Titan. *Journal of Geophysical Research: Space Physics*, *121*(3), 2095–2103. <https://doi.org/10.1002/2015JA022293>
- Shebanits, O., Wahlund, J. E., Edberg, N. J. T., Cray, F. J., Wellbrock, A., Andrews, D. J., et al. (2016). Ion and aerosol precursor densities in Titan's ionosphere: A multi-instrument case study. *Journal of Geophysical Research: Space Physics*, *121*(10). <https://doi.org/10.1002/2016JA022980>
- Simon, S., Treeck, S. C., Wennmacher, A., Saur, J., Neubauer, F. M., Bertucci, C. L., & Dougherty, M. K. (2013). Structure of Titan's induced magnetosphere under varying background magnetic field conditions: Survey of Cassini magnetometer data from flybys TA-T85. *Journal of Geophysical Research: Space Physics*, *118*(4), 1679–1699. <https://doi.org/10.1002/jgra.50096>
- Simon, S., Wennmacher, A., Neubauer, F. M., Bertucci, C. L., Kriegel, H., Russell, C. T., & Dougherty, M. K. (2010). Dynamics of Saturn's magnetodisk near Titan's orbit: Comparison of Cassini magnetometer observations from real and virtual Titan flybys. *Planetary and Space Science*, *58*(12), 1625–1635. <https://doi.org/10.1016/j.pss.2010.08.006>
- Sonnerup, B. U. Ö., & Scheible, M. (1998). Minimum and maximum variance analysis. In *ISSI Scientific Reports Series* (Vol. 1, pp. 185–220).
- Stasiewicz, K., Bellan, P., Chaston, C., Kletzing, C., Lysak, R., Maggs, J., et al. (2000). Small scale Alfvénic structure in the aurora. *Space Science Reviews*, *92*(3/4), 423–533. <https://doi.org/10.1023/a:1005207202143>
- Szegő, K., Glassmeier, K.-H., Bingham, R., Bogdanov, A., Fischer, C., Haerendel, G., & Zank, G. (2000). Physics of mass loaded plasmas. *Space Science Reviews*, *94*(3/4), 429–671. <https://doi.org/10.1023/A:1026568530975>
- Treumann, R. A., & Baumjohann, W. (1997). Advanced space plasma physics. <https://doi.org/10.1142/p020>
- Vuitton, V., Yelle, R. V., & McEwan, M. J. (2007). Ion chemistry and N-containing molecules in Titan's upper atmosphere. *Icarus*, *191*(2), 722–742. <https://doi.org/10.1016/j.icarus.2007.06.023>
- Wahlund, J.-E., Modolo, R., Bertucci, C., & Coates, A. J. (2014). Titan's magnetospheric and plasma environment. In I. Müller-Wodarg, C. A. Griffith, E. Lellouch, & T. E. Cravens (Eds.), *Titan: Interior, surface, atmosphere, and space environment* (pp. 419–458). Cambridge University Press.
- Waite, J. H., Niemann, H., Yelle, R. V., Kasprzak, W. T., Cravens, T. E., Luhmann, J. G., et al. (2005). Ion neutral mass spectrometer results from the first flyby of Titan. *Science*, *308*(5724), 982–986. <https://doi.org/10.1126/science.1110652>
- Waite, J. H., & Wilson, R. J. (2022). *Cassini-Huygens plasma spectrometer (CAPS) calibrated data bundle*. NASA Planetary Data System. urn:nasa:pds:cassini-caps-calibrated:1.0. <https://doi.org/10.17189/CM56-W882>
- Wei, H. Y., Russell, C. T., Dougherty, M. K., Ma, Y. J., Hansen, K. C., McAndrews, H. J., et al. (2011). Unusually strong magnetic fields in Titan's ionosphere: T42 case study. *Advances in Space Research*, *48*(2), 314–322. <https://doi.org/10.1016/j.asr.2011.02.009>
- Wei, H. Y., Russell, C. T., Dougherty, M. K., Neubauer, F. M., & Ma, Y. J. (2010). Upper limits on Titan's magnetic moment and implications for its interior. *Journal of Geophysical Research*, *115*(E10), E10007. <https://doi.org/10.1029/2009JE003538>
- Wellbrock, A., Coates, A. J., Jones, G. H., Lewis, G. R., & Waite, J. H. (2013). Cassini CAPS-ELS observations of negative ions in Titan's ionosphere: Trends of density with altitude. *Geophysical Research Letters*, *40*(17), 4481–4485. <https://doi.org/10.1002/grl.50751>
- Wellbrock, A., Coates, A. J., Sillanpää, I., Jones, G. H., Arridge, C. S., Lewis, G. R., et al. (2012). Cassini observations of ionospheric photoelectrons at large distances from Titan: Implications for Titan's exospheric environment and magnetic tail. *Journal of Geophysical Research*, *117*(A3), A03216. <https://doi.org/10.1029/2011JA017113>
- Yao, Z., Dunn, W. R., Woodfield, E. E., Clark, G., Mauk, B. H., Ebert, R. W., et al. (2021). Revealing the source of Jupiter's x-ray auroral flares. *Science Advances*, *7*(28), eabf0851. <https://doi.org/10.1126/sciadv.abf0851>
- Young, D. T., Berthelier, J. J., Blanc, M., Burch, J. L., Coates, A. J., Goldstein, R., et al. (2004). Cassini plasma spectrometer investigation. *Space Science Reviews*, *114*(1–4), 1–112. <https://doi.org/10.1007/s11214-004-1406-4>